miR-631 targets the oncogene *RAB11A*: implications for oral squamous cell carcinoma pathogenesis and therapeutics

Harsha Pulakkat Muralidharan[1*], Radha Mishra[1], Champaka Gopal[2] and Arun Kumar[1*]

[1]Department of Developmental Biology and Genetics, Indian Institute of Science, Bangalore 560012, India; [2]Department of Pathology, Kidwai Memorial Institute of Oncology, Bangalore 560029, India

*Joint corresponding authors:

Email ID: harshapm@iisc.ac.in (HPM)

Email ID: arunk@iisc.ac.in (AK)

Short title: miR-631 targets *RAB11A*

Abstract

Despite technological advancements, the five-year survival rate for oral squamous cell carcinoma (OSCC) remains low, highlighting the urgent need to develop more effective therapies. With this objective, we intended to identify the potential therapeutic tumor suppressor microRNAs (miRs) in OSCC. In a previous work from our laboratory, we treated OSCC cells with 5-Azacytidine, a global DNA methyltransferase inhibitor, and subsequently performed a microRNA microarray analysis and identified 50 upregulated miRs. Of these, miR-631 that had no previously known roles in OSCC was selected for the further analysis in the present study. Our experiments show that miR-631 reduces proliferation of OSCC cells and binds to the 3'UTR of the oncogene *RAB11A* and reduces its expression at both the transcript and protein levels. The upregulation of miR-631 is shown to be due to its promoter demethylation after the 5-Azacytidine treatment. We demonstrate that miR-631 inhibits proliferation and anchorage-independent growth in soft agar and increases apoptosis of OSCC cells, in part, via targeting *RAB11A*. The inverse correlation in the levels of miR-631 and *RAB11A* in various cancer cell lines and in a majority (58.33%) of OSCC patient samples suggests the biological relevance of their interaction. The nude mice OSCC xenograft study suggests the tumor suppressive nature of miR-631. Further, miR-631 and *RAB11A* interaction reduces the Wnt signaling in OSCC. Based on our results, we propose that miR-631 functions as a tumor suppressor and holds promise as a potential therapeutic agent for treating OSCC.

Key words: microRNAs; tumor suppressor; miR-631; *RAB11A*; OSCC; oral cancer.

Introduction

Oral squamous cell carcinoma (OSCC) or oral cancer, a predominant malignancy of the epithelial layer of the oral cavity, accounts for a staggering 90% of all oral cancers [1]. Alarmingly, the Global Cancer Observatory reported 377,713 cases of OSCC in 2020, with a projected 40% rise by 2040 [GLOBOCAN 2022; https://gco.iarc.fr/]. In India, oral cancer ranks as the most common cancer in males and the fourth most common cancer in females [GLOBOCAN 2022; https://gco.iarc.fr/]. Despite advancements, the five-year survival rate for OSCC remains dismally below 50%, underscoring the urgent need for more effective therapeutic strategies [2]. OSCC is driven by a range of risk factors, including tobacco and alcohol consumption, smoking, betel quid chewing [3], HPV 16 or HPV 18 infections [4], nutrient deficiencies [5], genetic susceptibility, and poor oral hygiene [6].

Current treatment strategies for OSCC primarily rely on combinations of surgery, radiation therapy, chemotherapy, immunotherapy, and targeted approaches, such as EGFR inhibitors like cetuximab [7]. While these methods have improved outcomes to some extent, the search for innovative therapies continues. In this context, microRNAs (miRs) have emerged as promising therapeutic agents across various diseases. These small, non-coding RNA molecules, typically ~18-25 nucleotides long, are transcribed by RNA polymerases II and III and regulate gene expression by binding to complementary sequences in target genes [8]. miRs influence diverse cellular processes, including cell-cell communication, development, immune responses, epigenetic regulation, circadian rhythms, and hallmarks of cancer [9]. Most commonly, they target the 3' untranslated regions (3'UTRs) of genes to inhibit translation or to degrade the RNA transcripts. However, their versatility extends further. Our group has recently demonstrated that miR-617 can activate gene expression by binding to the promoter region of *DDX27* [10]. miRs have also been shown to modulate gene expression by interacting with coding regions or 5'UTRs [9,11]. The therapeutic potential of miRs is already being explored in various diseases. For example, miR-155, miR-21, miR-92, and miR-16 have shown promise in treating T-cell lymphoma, Alport syndrome, wound healing, and mesothelioma, respectively [12]. Notably, miR-122 has advanced to phase II clinical trials for Hepatitis C treatment [12], thus further highlighting the transformative potential of these molecules in modern medicine.

miRs can act either as oncomiRs, which positively regulate oncogenes, or as tumor suppressor miRs, which negatively regulate oncogenes. A previous study from our laboratory

has revealed that miR-155 functions as an oncomiR in OSCC by negatively regulating the *CDC73* tumor suppressor gene [13]. Recent studies from our laboratory showed how tumor suppressor miR-6741-3p and miR-198 target *SRSF3* and *TOPORS* genes, respectively, in OSCC [14, 15]. The action of miRs is highly context- and tissue-specific. Factors such as the amplification or deletion of miR genes, defects in miR biogenesis pathways, alterations in miR transcription control, and dysregulated epigenetic modifications can contribute to cancer development [16]. Smoking and alcohol consumption, the two primary risk factors for oral cancer, are known to influence the epigenetic regulation of several protein-coding genes and miRs directly associated with OSCC development [17]. Many miRs are epigenetically dysregulated in OSCC [18]. Further, OSCC patient tissue samples exhibit higher levels of gene hypermethylation compared to their normal counterparts [19]. Hypermethylation of gene promoters, a hallmark of epigenetic regulation, can silence gene expression [10, 15]. When tumor suppressor genes are affected, this silencing directly contributes to tumor development. Encouragingly, reversing such methylation patterns can reactivate these critical genes, offering a potential therapeutic strategy [20]. In a similar vein, miR genes with tumor-suppressive potential are also susceptible to hypermethylation in cancer cells. Profiling the methylation status of miRs in OSCC could uncover novel tumor suppressors, paving the way for innovative diagnostic and therapeutic approaches. With this rationale, a previous study by our group treated cells from an OSCC cell line SCC131 with 5-Azacytidine, a DNA methyl transferase (DNMT) inhibitor, and using the microRNA microarray analysis of probes for 2,549 microRNAs showed the upregulation of 50 miRs and the downregulation of 28 miRs, including the upregulation of miR-631 with a significant fold change of 4.39 [14]. Given the upregulation in the microRNA microarray analysis [14], we conducted further experiments to validate the role of miR-631 as a tumor suppressor in OSCC and explored its potential as a therapeutic target for this disease. Further, this study also investigated the mechanism behind its upregulation in OSCC cells treated with 5-Azacytidine, impact on various cancer hallmarks, biological relevance using patient tumor samples, potential target genes as well as therapeutic potential, using a xenograft nude mouse model.

Results

Validation of miR-631 upregulation in SCC131 cells post 5-Azacytidine treatment

As expected, the qRT-PCR analysis showed a significant upregulation of miR-631 in 5-Azacytidine treated SCC131 cells compared to those treated with the control (DMSO), thereby validating the microarray data **(S1A Fig)**. The semi-quantitative RT-PCR analysis also showed a similar result **(S1B Fig)**.

miR-631 overexpression reduces proliferation of OSCC cells

miRs with tumor suppressive potential are often downregulated in cancer. Since miR-631 expression increased in SCC131 cells after the 5-Azacytidine treatment, we aimed to determine if it has a tumor suppressive nature. For this purpose, miR-631 was first cloned in the pcDNA3-EGFP vector to generate the pmiR-631 construct. The effect of miR-631 on cell proliferation was then analyzed by transiently transfecting pcDNA3-EGFP and pmiR-631 separately in cells from SCC131 and SCC084 OSCC cell lines, and the cell proliferation was assessed by the trypan blue dye exclusion assay. Both SCC131 and SCC084 cells showed reduced cell proliferation over the period of 4 days upon transfection with pmiR-631 in comparison to those transfected with the vector **(S2A Fig)**. The effect of miR-631 on cell proliferation was further confirmed by the BrdU incorporation assay in cells from both cell lines **(S2B Fig)**. The results showed that miR-631 significantly reduces proliferation of cells from both cell lines transfected with pmiR-631 as compared to those transfected with the vector (**S2 Fig**).

Demethylation of the *MIR631* promoter causes miR-631 upregulation post 5-Azacytidine treatment of cells

Since miR-631 was upregulated following the 5-Azacytidine treatment, we hypothesized that this might be due to the removal of methylation from the *MIR631* promoter. Since the promoter for this intronic miR remains uncharacterized, we first sought to characterize the promoter of the *MIR631* gene, which is located in an intron between exons 5 and 6 in the antisense strand of the host gene *NEIL1* (Nei like DNA glycosylase 1) on chromosome 15 **(S3 Fig)**. The direction of transcription for *MIR631* is opposite to the host gene *NEIL1* **(S3 Fig)**. Based on the bioinformatic prediction using the DBTSS, Promoter 2.0 and Alggen Promo databases, a putative *MIR631* promoter sequence was retrieved **(S4 Fig)**, which was then cloned in the pGL3-Basic vector to generate the pProm-MIR631 construct. pProm-

150 MIR631, pGL3-Control (positive control) and pGL3-Basic (negative control) were then
151 transiently transfected separately in SCC131 cells and the dual-luciferase reporter assay was
152 used to determine the promoter activity of the cloned *MIR631* sequence. The cloned *MIR631*
153 sequence in pProm-MIR631 showed an enhanced luciferase activity as compared to the pGL3-
154 Basic vector, suggesting that it represents the *MIR631* promoter **(Fig 1A)**. We then looked for
155 the methylation of a CpG-rich region in the *MIR631* promoter, using the sodium bisulfite PCR
156 sequencing **(Fig 1B)**. The results showed 70% methylation of CpG sites in 5-Azacytidine
157 treated cells compared to 98.60% methylation of CpG sites in DMEM-treated cells **(Fig 1C)**,
158 suggesting that the observed upregulation of miR-631 in 5-Azacytidine treated SCC131 cells
159 is due to demethylation of its promoter.
160
161 **Fig 1. Characterization of the *MIR631* promoter and deciphering the mechanism of miR-**
162 **631 upregulation in SCC131 cells. (**A) The dual-luciferase reporter assay shows an increased
163 luciferase activity for the putative promoter fragment cloned in pProm-MIR631. pGL3-Basic
164 is a promoter less vector, whereas pGL3-Control harbors the SV40 promoter and was used a
165 positive control. Each bar in the dual-luciferase reporter assay is an average of three technical
166 replicates. (B) Schematic representation of the *MIR631* promoter with a 212 bp long CpG
167 island harboring 14 CpG sites. Pre-miR-631 represents the location of the precursor sequence
168 of miR-631. (C) Schematic representation of the methylation pattern of the CpG island. Filled
169 circles represent methylated CpG sites, whereas empty circles represent non-methylated CpG
170 sites. Each line represents a single TA clone. *Abbreviations:* RLU, Relative light unit; Meth
171 Fp, Methylation specific forward primer; and, Meth Rp, Methylation specific reverse primer.
172
173 ***In silico* identification and qRT-PCR analysis of putative gene targets of miR-631**

174 miRs are known to exert their effects through target genes. Therefore, to select a target
175 gene for miR-631, five different target gene prediction tools were used: TargetScan, miRwalk,
176 DIANA, miRabel, and miRDB (**S1 Table**). We first focused on identifying target genes that
177 were commonly predicted by these tools **(S1 Table)** such as *AKR1B1* (Aldo-keto reductase
178 family member B1), *OASL* (Oligo adenyl synthase), *RAP1B* (Rab associated protein 1B),
179 *RAB11A* (Ras GTPase family member 11A) and *PTPRE* (Protein tyrosine phosphatase
180 receptor). *PTPRE* is already a known target of miR-631. We then also considered factors such
181 as the number of target sites present in the 3'UTR of each target gene, the predicted free energy
182 of binding between miR-631 and the target gene, and the accessibility of the target site for miR-

183 631 binding, using bioinformatics tools like STARFold [https://sfold.wadsworth.org/cgi-bin/],
184 and UNAFold [https://www.unafold.org/] (**S2 Table).** Finally, we selected the following two
185 potential target genes for further investigation: *RAB11A*, and *RAP1B*. To determine if miR-631
186 regulates these genes, we transfected pmiR-631 and the vector separately in SCC131 cells and
187 assessed their transcript levels (**Figs 2A and S5)**. The results showed that miR-631 regulates
188 the transcript level of *RAB11A* **(Fig 2A)**. miR-631 did not regulate the transcript level of *RAP1B*
189 (**S5 Fig**). As expected, *PTPRE* was found to be regulated by miR-631 **(S5 Fig)**. miR-631 also
190 regulated the protein level of RAB11A **(Fig 2A)**. To determine if there is dose-dependent
191 regulation of RAB11A by miR-631, we transfected different quantities of pmiR-631 in
192 SCC131 cells and assessed the levels of RAB11A transcript and protein **(Fig 2B)**. The results
193 showed that the levels of both transcript and protein of RAB11A decreases in a dose-dependent
194 manner with increasing quantities of pmiR-631 **(Fig 2B)**. Since miR-631 was found to be
195 upregulated following the 5-Azacytidine treatment of SCC131 cells, we next examined the
196 transcript and protein levels of RAB11A in 5-Azacytidine treated SCC131 cells **(Fig 2C)**. As
197 expected, the miR-631 level was upregulated and RAB11A transcript and protein levels were
198 downregulated in 5-Azacytidine treated cells compared to those treated with DMSO, further
199 suggesting that miR-631 regulates the level of RAB11A **(Fig 2C)**.

200 **Fig 2. Identification of *RAB11A* as a gene target for miR-631.** (A) Overexpression of miR-
201 631 using the pmiR-631 construct in SCC131 cells leads to reduced RAB11A transcript and
202 protein levels. (B) The dose-dependent regulation of RAB11A transcript and protein levels in
203 SCC131 cells with increasing quantities of pmiR-631. (C) Reduced levels of RAB11A
204 transcript and protein following the 5-Azacytidine treatment of SCC131 cells with the
205 concomitant increase in miR-631 levels. Each bar for qRT-PCR is an average of two technical
206 replicates.

207

208 **Confirmation of the direct interaction between miR-631 and 3'UTR of *RAB11A***

209 The bioinformatics analysis predicted the presence of a target site (TS) in the 3'UTR
210 of *RAB11A* for the seed region (SR) of miR-631 **(Fig 3A)**, suggesting a potential interaction
211 between them. Notably, the predicted TS for miR-631 showed conservation across different
212 species, as indicated by the TargetScan program **(Fig 3A).** We then used the dual-luciferase
213 reporter assay to experimentally verify the direct interaction between miR-631 and the 3'UTR
214 of *RAB11A* and therefore generated the following constructs in the pMIR-REPORT™ vector:
215 p3'UTR-RAB11A-S with the 3'UTR of *RAB11A* in a sense-orientation, p3'UTR-RAB11A-M

216 harboring the 3'UTR of *RAB11A* with mutated TS, and p3'UTR-PTPRE-S with the 3'UTR of
217 *PTPRE* in a sense-orientation. We also generated another construct for miR-631 (pmiR-631-
218 M) in the pcDNA3-EGFP vector in which the SR was mutated by the site-directed mutagenesis
219 **(Fig 3B)**. We then co-transfected different *RAB11A* 3'UTR constructs (e.g., p3'UTR-RAB11A-
220 S and p3'UTR-RAB11A-M) separately with the vector, pmiR-631 or pmiR-631-M in SCC131
221 cells and determined the luciferase activity. The cells co-transfected with p3'UTR-RAB11A-
222 S and pmiR-631 showed a significantly reduced luciferase activity as compared to those co-
223 transfected with p3'UTR-RAB11A-S and pcDNA3-EGFP **(Fig 3C)**. The cells co-transfected
224 with p3'UTR-RAB11A-M and pmiR-631 showed luciferase activity comparable to those co-
225 transfected with p3'UTR-RAB11A-S and pcDNA3-EGFP, due to the absence of a functional
226 TS in 3'UTR of *RAB11A* in the p3'UTR-RAB11A-M construct **(Fig 3C)**. Similarly, cells co-
227 transfected with p3'UTR-RAB11A-S and pmiR-631-M showed no difference in the luciferase
228 activity as compared to those co-transfected with p3'UTR-RAB11A-S and pcDNA3-EGFP
229 **(Fig 3C)**, due to the absence of SR in pmiR-631-M construct. As expected, the cells transfected
230 with p3'UTR-PTPRE-S and pmiR-631 showed a significantly reduced luciferase activity
231 compared to those co-transfected with p3'UTR-PTPRE-S and pcDNA3-EGFP **(Fig 3C)**. These
232 results suggested that the SR of miR-631 interacts directly with the TS of the 3'UTR of
233 *RAB11A* in a sequence-specific manner.

234 **Fig 3. Confirmation of a direct interaction between miR-631 and the 3'UTR of *RAB11A***
235 (A) Conservation of the putative TS in the 3'UTR of *RAB11A* across different species for the
236 SR of miR-631. (B) Schematic representation of the constructs used in the dual-luciferase
237 reporter assay. The X indicates abrogated TS or SR in a construct. (C) The dual-luciferase
238 reporter assay in SCC131 cells co-transfected with different constructs. Note, reduced RLU in
239 cells co-transfected with p3'UTR-RAB11A-S and pmiR-631 compared to those co-transfected
240 with the vector control and pmiR-631. Each bar is an average of three technical replicates.
241 *Abbreviations:* TS, Target Site; and SR, Seed Region.
242

243 **Overexpression of RAB11A increases proliferation of OSCC cells**

244 As previously discussed, miRs carry out their effects by targeting specific genes. Since
245 miR-631 reduces proliferation of both SCC131 and SCC084 cells, we wanted to determine the
246 role of its target gene *RAB11A* on cell proliferation. To investigate this, the pRAB11A construct
247 harboring the entire ORF of *RAB11A* and the cloning vector pcDNA3.1(+) were transiently
248 transfected separately in SCC131 and SCC084 cells and the cell proliferation was determined,

using the trypan blue dye exclusion method. The results revealed a significant increase in the proliferation of both SCC131 and SCC084 cells transfected with pRAB11A compared to those transfected with the vector, indicating the pro-proliferative role of *RAB11A* in OSCC **(S6A Fig).** The same hypothesis was further tested using the BrdU incorporation assay, and the absorbance values indicated that both SCC131 and SCC084 cells transfected with pRAB11A showed increased cell proliferation compared to those transfected with the vector, further confirming the pro-proliferative role of *RAB11A* **(S6B Fig)**.

Inverse correlation of miR-631 and *RAB11A* levels across various cancer cell lines and OSCC patient samples

Prior experiments have validated that miR-631 targets *RAB11A* and reduces its expression at both the protein and transcript levels. To comprehend the biological significance of the interaction of miR-631 and *RAB11A*, we assessed the expression of both miR-631 and *RAB11A*, using the qRT-PCR analysis in various cancer cell lines. In general, we observed an inverse correlation in the expression of miR-631 and its target gene *RAB11A* among the cell lines **(S7 Fig)**. For example, the level of miR-631 was reduced in A549 cells, whereas the level of *RAB11A* was increased in these cells **(S7 Fig)**.

We also assessed the expression levels of miR-631 and *RAB11A* in 36 matched normal oral tissue and OSCC patient samples by qRT-PCR **(S8 Fig)**. The miR-631 expression was downregulated in 11/36 patient samples [viz., patient samples 50, 52, 55, 56, 62, 64, 68, 72, 82, 86, and 90], and its level was upregulated in 17/36 samples [viz., patient samples 38, 41, 54, 58, 61, 66, 69, 71, 76, 77, 78, 79, 80, 81, 87, 88, and 89]. The *RAB11A* expression was upregulated in 13/36 patient samples [viz., 52, 55, 56, 57, 62, 64, 65, 68, 70, 76, 85, 89, and 90], whereas its levels was downregulated in 20/36 patient samples [viz., patient samples 38, 41, 50, 58, 61, 66, 69, 71, 72, 74, 75, 77, 78, 80, 81, 82, 83, 86, 87, and 88]. In 8/36 samples, miR-631 levels did not show any change [viz., patient samples 57, 63, 65, 70, 74, 75, 83, and 85]. The levels of *RAB11A* did not show any change in 3/36 patient samples [viz., patient samples 54, 63, and 79]. miR-631 was downregulated, whereas *RAB11A* was upregulated in 7/36 samples [viz., patient samples 52, 55, 56, 62, 64, 68, 90]. miR-631 showed upregulation and *RAB11A* showed downregulation in 14/36 samples [viz., patient samples 38, 41, 58, 61, 66, 69, 71, 74, 77, 78, 80, 81, 87, and 88]. Overall, 21/36 (58.33%) patient samples (viz. patient samples 38, 41, 52, 55, 56, 58, 61, 62, 64, 66, 68, 69, 71, 74, 77, 78, 80, 81, 87, 88 and 90)

280 showed an inverse correlation in the expression of miR-631 and *RAB11A* **(S8 Fig)**, suggesting
281 the physiological relevance of their interaction.

282 **Expression of *RAB11A* at the protein level is regulated by the presence of its 3'UTR**

283 As shown above, the reduced level of RAB11A results due to a direct binding of miR-
284 631 to the 3'UTR of *RAB11A* **(Fig 3)**. To investigate if the protein levels of RAB11A depend
285 on the presence or the absence of its 3'UTR, we used the following constructs: pRAB11A
286 harboring a complete *RAB11A* ORF without its 3'UTR, pRAB11A-UTR-S harboring a
287 complete ORF of *RAB11A* and its 3'UTR in a sense orientation, and pRAB11A-UTR-M
288 harboring a complete ORF of *RAB11A* with its 3'UTR with mutated TS **(Fig 4A)**. We then
289 transiently transfected the vector control [pcDNA3.1(+)] only or pRAB11A, pRAB11A-UTR-
290 S and pRAB11A-UTR-M separately with pmiR-631 in SCC131 and SCC084 cells and
291 assessed the levels of RAB11A protein by Western blotting **(Figs 4A and S9A)**. The results
292 showed that the RAB11A level is reduced in cells co-transfected with the vector and pmiR-631
293 compared to those transfected with the vector control only, because of miR-631 targeting the
294 endogenous *RAB11A* **(Figs 4A and S9A)**. An increased level of RAB11A was observed in
295 cells co-transfected with pmiR-631 and pRAB11A as compared to those co-transfected with
296 the vector and pmiR-631 **(Figs 4A and S9A)**. A reduced level of RAB11A was observed in
297 cells co-transfected with pRAB11A-UTR-S and pmiR-631 as compared to those co-transfected
298 with pRAB11A and pmiR-631, due to the presence of a functional TS in the 3'UTR of
299 pRAB11A-UTR-S **(Figs 4A and S9A)**. Further, an increased level of RAB11A was observed
300 in cells co-transfected with pRAB11A-UTR-M and pmiR-631 as compared with those co-
301 transfected with pRAB11A-UTR-S and pmiR-631, because of the absence of TS in the 3'UTR
302 of pRAB11A-UTR-M **(Figs 4A and S9A)**. These observations suggested that the RAB11A
303 expression depends on the presence or absence of its 3'UTR and is, in part, regulated by miR-
304 631.

305 **miR-631 regulates cancer hallmarks, in part, by targeting the 3'UTR of *RAB11A***

306 We then wanted to understand the effect of miR-631-mediated regulation of *RAB11A*
307 on a few hallmarks of cancer, such as cell proliferation, anchorage-independent growth, and
308 apoptosis. To this end, we co-transfected pRAB11A or pRAB11A-UTR-S, and pRAB11A-
309 UTR-M constructs separately with pmiR-631 in SCC131 and SCC084 cells and assessed cell
310 proliferation using both trypan blue dye exclusion (**Figs 4B and S9B**) and BrdU incorporation
311 (**Figs 4C and S9C**) assays. As expected, we observed a decreased rate of proliferation of cells

312 co-transfected with pmiR-631 and vector compared with those transfected with the vector only
313 **(Figs 4B, 4C, S9B and S9C)** due to targeting of endogenous *RAB11A* by miR-631. Further,
314 we observed a decreased rate of cell proliferation in cells co-transfected with pmiR-631 and
315 pRAB11A-UTR-S compared with those co-transfected with pmiR-631 and pRAB11A, due to
316 the presence of a functional TS in the 3'UTR of pRAB11A-UTR-S **(Figs 4B, 4C, S9B and**
317 **S9C)**. As expected, we observed no significant difference in the rate of proliferation of cells
318 co-transfected with pmiR-631 and pRAB11A compared with those co-transfected with pmiR-
319 631 and pRAB11A-UTR-M, due to the absence of a functional TS in 3'UTR of pRAB11A-
320 UTR-M. These observations highlighted the negative regulation of cell proliferation by miR-
321 631, in part, via targeting the 3'UTR of *RAB11A*.

322 **Fig 4. Regulation of *RAB11A* by miR-631 is mediated by its 3'UTR and the impact of this**
323 **regulation on proliferation of SCC131 cells. (**A) The RAB11A protein levels are dependent
324 on the presence or absence of a functional TS in its 3'UTR for miR-631. Schematic diagrams
325 of different *RAB11A* constructs are shown above the Western blots. (B) The negative regulation
326 of cell proliferation by miR-631, in part, via targeting the 3'UTR of *RAB11A*, using the trypan
327 blue dye exclusion assay. (B) The negative regulation of cell proliferation by miR-631, in part,
328 via targeting the 3'UTR of *RAB11A*, using the BrdU incorporation assay. Each datapoint is an
329 average of three values.
330

331 To investigate the effect of miR-631-mediated regulation of *RAB11A* on anchorage-
332 independent growth of OSCC cells, we transfected the vector only or co-transfected pRAB11A,
333 pRAB11A-UTR-S and pRAB11A-UTR-M separately with pmiR-631 in SCC084 and SCC131
334 cells and observed the colony formation ability by the soft agar colony-forming assay **(Figs 5A**
335 **and S10A)**. As expected, we observed a reduced number of colonies in cells co-transfected
336 with pmiR-631 and the vector compared with those transfected with the vector only **(Figs 5A**
337 **and S10A)**. Further, a reduced number of colonies was observed in cells co-transfected with
338 pmiR-631 and pRAB11A-UTR-S compared with those co-transfected with pRAB11A and
339 pmiR-631 **(Figs 5A and S10A)**, due to binding of miR-631 to the TS in the pRAB11A-UTR-
340 S. Further, no significant difference in the number of colonies was observed in cells co-
341 transfected with pmiR-631 and pRAB11A compared with those co-transfected with pmiR-631
342 and pRAB11A-UTR-M, due to the absence of a functional TS in pRAB11A-UTR-M **(Figs 5A**
343 **and S10A)**. These results clearly suggested a negative regulation of miR-631 on the anchorage-
344 independent growth, in part, by targeting the 3'UTR of *RAB11A*.

345 To determine if miR-631 regulates apoptosis by targeting the 3'UTR of *RAB11A*, we
346 transfected the vector only or co-transfected pRAB11A, pRAB11A-UTR-S and pRAB11A-
347 UTR-M separately with pmiR-631 in SCC084 and SCC131 and performed caspase-3 assay
348 **(Figs 5B and S10B)**. We observed a significant increase in the rate of apoptosis in cells co-
349 transfected with pmiR-631 and the vector compared with those transfected with the vector only
350 **(Figs 5B and S10B)**. The percentage of caspase-3 positive cells was significantly higher in
351 cells transfected pmiR-631 and the vector compared with those co-transfected with pRAB11A
352 and pmiR-631, due to ectopic expression of oncogenic *RAB11A* **(Figs 5B and S10B)**. Further,
353 no significant difference in the percentage of caspase-3 positive cells was observed in cells co-
354 transfected with pmiR-631 and pRAB11A compared with those co-transfected with pmiR-631
355 and pRAB11A-UTR-M, due to the absence of a functional TS in pRAB11A-UTR-M **(Figs 5B**
356 **and S10B)**. These observations suggested that miR-631 positively regulates apoptosis of
357 SCC131 and SCC084 cells, in part, by directly targeting the 3'UTR of *RAB11A*.

358 **Fig. 5. Regulation of anchorage-independent growth and apoptosis by miR-631, in part,**
359 **via targeting the 3'UTR of *RAB11A* in SCC131 cells.** (A) The negative regulation of
360 anchorage-independent growth by miR-631, in part, via targeting the 3'UTR of *RAB11A.*
361 Representative microphotographs of the colonies for SCC131 cells co-transfected with pmiR-
362 631 and different *RAB11A* overexpression constructs or vector control from the soft agar
363 colony-forming assay are shown on the right. The bar represents 100 nm. (B) The positive
364 regulation of apoptosis by miR-631, in part, via targeting the 3'UTR of *RAB11A.* Each
365 datapoint is an average of three values.

366 **Role of the miR-631/*RAB11A* axis in regulating Wnt signaling in OSCC cells**

367 One of the aberrant pathways implicated in oral cancer is the Wnt signaling pathway
368 [21]. To gauge the activation of Wnt signaling, a gold-standard reporter assay employing the
369 TOPflash reporter construct (TCF Reporter Plasmid) was used. This construct incorporates a
370 minimal fos promoter coupled to TCF-binding sites upstream to the firefly luciferase gene.
371 When the Wnt signaling is activated, the luciferase activity increases due to the greater amount
372 of beta-catenin binding to the TCF site. In our study, we assessed the luciferase activity
373 following the overexpression of pRAB11A or pmiR-631 in both SCC131 and SCC084 cells
374 **(S11 Fig)**. The results revealed a significant increase in the luciferase activity with RAB11A
375 overexpression **(S11A Fig)**, whereas miR-631 overexpression led to a reduced luciferase

activity **(S11B Fig)**. These experiments confirmed the activation of Wnt signaling in OSCC cells by RAB11A, which was diminished when miR-631 was overexpressed **(S11 Fig)**.

To determine whether RAB11A-mediated Wnt signaling activation in OSCC cells is regulated by miR-631, we employed the same *RAB11A* constructs (i.e., pRAB11A, pRAB11A-UTR-S and pRAB11A-UTR-M) used earlier. We co-transfected SCC131 cells with the TOPflash reporter plasmid and pmiR-631 or TOPflash reporter plasmid and vector and determined the luciferase activity. The results showed a decreased luciferase activity in cells co-transfected with the TOPflash reporter plasmid and pmiR-631 compared to those co-transfected with the TOPflash reporter plasmid and vector **(S12 Fig)**. A significantly increased luciferase activity was observed in cells co-transfected with TOPflash, pmiR-631 and pRAB11A compared to those co-transfected with TOPflash and pmiR-631, suggesting that RAB11A enhances the Wnt signaling **(S12 Fig)**. However, the luciferase activity decreased in SCC131 cells co-transfected with TOPflash, pRAB11A-UTR-S and pmiR-631 compared to those co-transfected with TOPflash, pRAB11A-UTR-M and pmiR-631 **(S12 Fig).** This resulted due to the absence of miR-631 TS in the pRAB11A-UTR-M construct. The above observations suggested that RAB11A contributes to OSCC progression by enhancing Wnt signaling. Conversely, miR-631 acts as a negative regulator of Wnt signaling at least, in part, by targeting *RAB11A.* Similar results were observed in SCC084 cells as well **(S12 Fig)**.

miR-631 synthetic mimic suppresses *in vivo* tumor growth in nude mice

Since miR-631 showed anti-proliferative role in OSCC, we then wanted to investigate the efficacy of a synthetic mimic of miR-631 in reducing OSCC xenografts in nude mice. To achieve this, we first optimized the dosage of a synthetic miR-631 mimic in reducing RAB11A levels in SCC131 cells. To this end, we first transfected increasing quantities of the miR-631 mimic in SCC131 cells and assessed the levels of miR-631 and RAB11A **(S13 Fig)**. Notably, all the three quantities of the mimic (i.e., 200 nM, 400 nM and 600 nM) demonstrated a significant decrease in both RAB11A transcript and protein levels, accompanied by a corresponding increase in miR-631 transcript levels **(S13 Fig)**. We then chose the 400 nM of the synthetic miR-631 mimic as the dosage for the subsequent experiments in nude mice **(S13 Fig)**.

To determine if the synthetic miR-631 mimic reduces OSCC xenografts in nude mice, we transfected SCC131 cells with both the miR-631 mimic and a mimic control separately. Post 24 hr of transfection, we injected equal number of cells from each transfection in both

408 flanks of three female nude mice in each group, i.e., control mimic and synthetic miR-631 **(Fig**
409 **6A)**. Tumor growth was monitored for 23 days post-injection. As expected, there was a
410 significant reduction in weight and volume of OSCC xenografts in the group treated with the
411 synthetic miR-631 mimic compared to those in the control group **(Fig 6B)**. We also excised
412 the xenografts from the mice on Day 23, and determined the levels of miR-631 and RAB11A
413 to see if the synthetic miR-631 mimic is able to reduce the levels of RAB11A transcript and
414 protein. The results showed that the levels of both RAB11A transcript and protein are reduced
415 in OSCC xenografts treated with the miR-631 mimic compared to those treated with the control
416 mimic **(Fig 6C)**. These findings confirm that miR-631 acts as a tumor suppressor in OSCC.

417 **Fig 6. The effect of a synthetic miR-631 mimic on SCC131 cells-derived xenografts in**
418 **nude mice. (**A) Top panel: Photographs of nude mice showing tumor growth on Day 23 of
419 injection of cells pre-treated with a synthetic miR-631 Mimic (MM) or Mimic Control (MC).
420 Bottom Panel: Excised xenografts from each mouse on Day 23. Xenografts are circled by red
421 dash lines and labelled Left (L) and Right (R) according to the flanks they were excised from.
422 Note, there was no tumor formation in nude mouse, MC3. (B) Effect of a synthetic miR-631
423 mimic on tumor volumes during a time course of 7-23 days, and overall tumor weight of
424 xenografts on Day 23. (C) qRT-PCR and Western blot analyzes of excised xenografts from the
425 miR-631 mimic and the mimic control groups. Note, increased levels of miR-631 (Top panel)
426 are correlated with reduced levels of RAB11A (Bottom panel) in xenografts with the miR-631
427 mimic as compared to those with the mimic control.
428
429
430
431
432
433
434
435
436
437

438 **Discussion**

439 Studies have shown that miR-631 functions as a tumor suppressor in multiple cancers
440 [22-26]. For example, miR-631 targets the 3'UTR of the *PTPRE* oncogene in hepatocellular
441 carcinoma, whereas it targets the *ZAP70* oncogene in prostate cancer to inhibit invasion and
442 migration of prostate cancer cells [22, 23]. In the context of multiple myeloma, miR-631 targets
443 and downregulates the *UBCH10* gene [24]. It re-sensitizes doxorubicin-resistant
444 chondrosarcoma cells by targeting the *APLN* gene [25]. It also targets the *E2F2* gene in non-
445 small cell lung carcinoma and inhibits the PI3K-AKT signaling pathway [26]. Additionally, it
446 plays important roles in female reproductive physiology, and polymorphisms associated with
447 miR-631 are linked to recurrent implantation failure [27]. Bioinformatic predictions indicate
448 that it is differentially expressed in ovarian carcinoma and is predicted to be downregulated in
449 medulloblastoma as well [28, 29]. Our study has shown that miR-631 reduces proliferation of
450 OSCC cells and OSCC xenografts in nude mice, thus further strengthening its potential as a
451 tumor suppressor **(Figs S2 and 6)**. Thus, miR-631 is another tumor suppressor microRNA in a
452 growing list of tumor suppressor microRNAs that play a role in the pathogenesis of OSCC such
453 as let-7a, let-7b, let-7c, let-7d, let-7e, let-7f, let-7g, let-7i, miR-26a, miR-99a-5p, miR-137,
454 miR-139-5p, miR-143-3p, miR-184, miR-375, miR-617, miR-198, miR-6741-3p [10, 14, 15,
455 18].

456 The upregulation of miR-631 in SCC131 cells following the 5-Azacytidine treatment
457 could be due to one of the two possibilities: 1) demethylation of the *MIR631* gene promoter or
458 2) demethylation of the promoter of a transcriptional factor, which upon upregulation, binds to
459 the *MIR631* promoter and upregulates its expression. To investigate the first possibility, we
460 characterized the *MIR631* promoter and assessed its methylation pattern in 5-Azacytidine-
461 treated and untreated cells, using sodium bisulfite sequencing **(Fig 1)**. The analysis showed
462 reduced methylation across 14 CpG sites in the *MIR631* promoter in the 5-Azacytidine-treated
463 cells compared to untreated cells **(Fig 1)**, suggesting that the demethylation of the *MIR631*
464 promoter causes its upregulation in SCC131 cells. The demethylation of two other tumor
465 suppressor miR-617 and miR-198 promoters has also been shown to cause their upregulations
466 in OSCC cells following the 5-Azacytidine treatment [10, 16].

467 Each miR exerts its effect through multiple target genes, making its role context-
468 specific and tissue-specific. But in the context of OSCC, there are no known targets for miR-
469 631. We shortlisted predicted target genes for miR-631 using five miR target gene prediction

470 tools and focused on those that are commonly identified across all tools for further analysis.
471 After a detailed analysis using various bioinformatic tools as mentioned earlier and *in vitro*
472 assays, *RAB11A* was observed to be the direct target of miR-631 **(Fig 3C)**. We found that miR-
473 631 reduces RAB11A transcript and protein levels in a dose-dependent manner **(Fig 2B).** Since
474 miR-631 shows upregulation post 5-Azacytidine treatment, we also confirmed that the same
475 treatment renders RAB11A levels down because of its upregulation **(Fig 2C)**.

476 *RAB11A* is a member of Ras associated GTPase family and is located on chromosome
477 15q22.31 **(S3 Fig)**. It is a known oncogene with roles in skin cancer, NSCLC, breast cancer,
478 pancreatic cancer, and gastric cancer [30, 31]. In the context of breast cancer, miR-320a, and
479 miR-452 are shown to downregulate the expression of *RAB11A* to control tumor progression
480 [32, 33]. RAB11A upregulates YAP and Cyclins in NSCLC, whereas it upregulates p-Akt in
481 gastric cancer [30, 31]. In case of ovarian cancer, RAB11A is downregulated by miR-193a-5p
482 [34]. However, it was recently shown in head and neck carcinoma that RAB11A suppresses
483 cancer progression by regulating EGFR recycling and epithelial cell adhesion molecule
484 (EpCAM) exosome secretion in cells [35]. As a previously established oncogene having no
485 characterized functions known in OSCC, we looked further at the role of *RAB11A* in OSCC.
486 The effect of RAB11A on the cell proliferation was assessed by overexpressing the *RAB11A*
487 ORF in SCC131 and SCC084 cells. As expected, RAB11A was shown to increase the rate of
488 proliferation of OSCC cells, indicating its pro-proliferative nature, which is a known feature of
489 oncogenes **(S6 Fig)**.

490 To analyze the biological relevance of the interaction between miR-631 and *RAB11A*,
491 we assessed their transcript levels in different cancer cell lines such as U2Os, A549, HeLa,
492 Ln229 and MDA-MB-231 along with SCC131 and SCC084. A549 and U2Os with the lowest
493 levels of miR-631 showed higher expression levels of *RAB11A,* whereas Ln229 and MB-231
494 with comparatively higher levels of miR-631 showed reduced levels of *RAB11A* **(S7 Fig)**.
495 Thus, in general, an inverse correlation was observed in the expression pattern of miR-631 and
496 *RAB11A* across the cell lines **(S7 Fig)**. Similar analysis was also conducted in 36 matched
497 normal oral tissue and OSCC patient samples **(S8 Fig)**. Of the 36 patient samples, 21 (58.33%)
498 showed an inverse correlation in the expression levels of miR-631 and *RAB11A*, suggesting the
499 physiological relevance of their interaction **(S8 Fig)**. However, no inverse correlation in their
500 expression levels was observed in rest of the OSCC samples **(S8 Fig)**. We believe that this
501 could be due to tumor heterogeneity, redundancy of splicing factors, additional regulatory
502 levels of *RAB11A*, variable etiopathogenesis, and the heterogeneous genetic constitution of

503 each patient [36, 37]. Similar inconsistencies in expression levels of miRs and their target genes
504 have also been reported by other studies [10, 14, 15, 38].

505 Given the potential for multiple miRNAs to regulate a single gene target, we
506 specifically investigated whether the observed regulation results from a direct interaction
507 between miR-631 and the 3'UTR of *RAB11A*. It was found that miR-631 exerts its regulation
508 on RAB11A levels only when the target site is present in the 3'UTR of *RAB11A* **(Figs 3, 4A,**
509 **and S9A)**, and when the target site was mutated, RAB11A levels were not regulated by miR-
510 631 **(Figs 3, 4A and S9A)**. Since the anti-proliferative nature of miR-631 and pro-proliferative
511 nature of RAB11A are already shown by our experiments **(Figs S2 and S6)**, we then wanted
512 to check the effect of their interaction on a few hallmarks of cancer such as cell proliferation,
513 anchorage-independent growth, and apoptosis. Both trypan blue dye exclusion cell
514 proliferation and BrdU incorporation assays showed that miR-631 regulates proliferation of
515 both SCC131 and SCC084 cells, in part, via targeting the 3'UTR of *RAB11A* **(Figs 4B, 4C,**
516 **S9B** and **S9C)**. Another interesting cancer hallmark we investigated was the ability of cancer
517 cells to form colonies when grown in a soft agar growth medium, which indicated their
518 potential to grow in an anchorage-independent manner. Even this potential was enhanced by
519 RAB11A, whereas miR-631 reduced anchorage-independent growth **(Figs 5A and S10A)**, in
520 part, by targeting the 3'UTR of *RAB11A*. Further, miR-631 as a tumor suppressor increased
521 cellular apoptosis in both SCC131 and SCC084 cells, in part, by targeting the 3'UTR of
522 *RAB11A* **(Figs 5B and S10B)**. RAB11A is already known for its potential in promoting cancer
523 progression hallmarks in other cancers such as breast, gastric, and ovarian cancers [29-33]. Our
524 study thus further supports these observations.

525 Since miR-631 targets *RAB11A* in its downstream functions, we therefore looked for
526 the different pathways this interaction could be impacting. It was previously shown that
527 RAB11A promotes Wnt signaling pathway and aids in cancer progression in pancreatic cancer
528 [39]. As Wnt signaling has not been studied in OSCC so far, we went ahead and checked the
529 activation of Wnt signaling in SCC131 and SCC084 cells, using the TOPFlash Wnt reporter
530 plasmid [40]. The Wnt activation was analyzed in the overexpression background of *RAB11A*,
531 and it was found to be upregulated **(S11 Fig)**. However, upon miR-631 overexpression, the
532 Wnt activation was significantly reduced, indicating that miR-631 downregulates Wnt
533 Signaling by binding to the 3'UTR of *RAB11A*, and this regulation was reduced when the target
534 site of miR-631 was mutated **(S12 Fig)**. It was shown in a previous study that RAB11A sustains
535 Wnt signaling in pancreatic cancer [39], and it mediates the proliferation and motility of

536 esophageal cancer cells through Wnt signaling [41]. In OSCC, Wnt signaling is a widely
537 dysregulated biomolecular pathway [42]. For example, it was shown that an increased WNT5A
538 expression in the tumor tissue is likely to promote progression of OSCC [42]. Also,
539 overexpression of *β*-catenin promoted cisplatin resistance in OSCC in *vitro* and *in vivo* [43].
540 Further, many Wnt ligands such as WNT1, WNT3A, WNT7B, WNT11, FZD7, TCF4,
541 DKK1/2/3, and SFRP1/2/4/5 are known to be dysregulated in OSCC [21]. However, the
542 present study is the first one to explore the effect of RAB11A on Wnt signaling in the context
543 of OSCC.

544 Since the discovery of microRNA molecules as potential targets for cancer therapy,
545 studies have investigated their applications in cancer treatment [14, 15, 44]. Synthetic miR
546 mimics are artificially designed small RNA molecules that replicate the function of endogenous
547 microRNAs. However, they undergo chemical modifications to enhance stability and reduce
548 degradation. These modifications primarily involve replacing the 2′-hydroxy group of ribose
549 with fluoro (F) or methoxy (OMe) residues to prevent nucleolytic degradation and improve
550 duplex stability as well as substituting phosphodiester bonds with a phosphorothioate moiety
551 to resist DNase cleavage [44]. In cancers, a tumor suppressor miR mimic can bind to its
552 oncogene targets and suppress their action [45]. Since miR-631 was shown to be a tumor
553 suppressor in OSCC and one of its target genes is an oncogene *RAB11A*, we wanted to assess
554 its tumor suppressive potential in *in vivo* OSCC xenograft nude mouse model, using a synthetic
555 miR-631 mimic. The results showed that the miR-631 mimic reduces tumor weight and growth
556 of OSCC xenografts in nude mice **(Fig 6)**, and thus confirming that miR-631 is indeed a tumor
557 suppressor in OSCC, and it can be used for developing a potential therapeutic agent for OSCC,
558 and perhaps other cancers as well. In a systemic mouse model for non-small cell lung cancer,
559 introduction of tumor suppressor miR-34a mimic led to decrease in tumor burden [46].
560 Relevant tumor growth inhibition and survival improvement were observed in nude mice
561 bearing *TP53*-mutated multiple myeloma xenografts treated with miR-34a mimics [46]. More
562 et al. [14] have recently shown that the tumor suppressor miR-6741-3p mimic reduces size and
563 weight of OSCC xenografts in nude mice. Further, Sarkar et al. [15] have showed that a miR-
564 617 synthetic mimic reduces size and weight of OSCC xenografts in nude mice. Similarly,
565 miR-198 mimic also reduces size and weight of OSCC xenografts in nude mice [15].

566 In summary, our study is the first to establish the tumor-suppressive role of miR-631 in
567 OSCC, demonstrating its ability to regulate key cancer hallmarks, modulate Wnt signaling, and
568 suppress tumor growth in nude mice, in part, by targeting the oncogene *RAB11A*. We have

identified promoter methylation as the primary cause of miR-631 downregulation in OSCC and observed an inverse correlation in expression levels of miR-631 and *RAB11A* in various cancer cell lines and OSCC patient samples, suggesting the physiological relevance of their interaction. Further, the present study highlights the potential of miR-631 as a future therapeutic target for OSCC.

Materials and methods

Cell lines

The cell lines, UPCI: SCC131 and UPCI: SCC084, used in this study are a kind gift from Dr. Susanne M. Gollin (University of Pittsburgh, Pittsburgh, PA, USA) [47] and also purchased from the Leibniz institute DSMZ (http://www.dsmz.de). A549 cells were procured from Prof. Upendra Nongthomba's laboratory, Department of Developmental Biology and Genetics, Indian Institute of Science (IISc), Bangalore. U2Os cells were obtained from Prof. Ganesh Nagaraju's laboratory, Department of Biochemistry, IISc, Bangalore. MB-231 cells were obtained from Dr. Ramray Bhat's laboratory, Department of Developmental Biology and Genetics, IISc, Bangalore. HeLa cells were obtained from Dr. Sachin Kotak's laboratory, Department of Microbiology and Cell Biology, IISc, Bangalore. Ln229 was obtained from Prof. Kumaravel Somasundaram's laboratory Department of Microbiology and Cell Biology, IISc, Bangalore.

In silico identification of targets for miR-631

Five gene target prediction programs, namely miRDB [48; https://mirdb.org/cgi-bin/search.cgi], DIANA-microT-CDS [49; https://dianalab.ece.uth.gr/html/dianauniverse/index.php?r=microT_CDS], miRwalk [50; http://mirwalk.umm.uni-heidelberg.de/], miRabel [51; http://bioinfo.univ-rouen.fr/mirabel/view/result.php?page=mir], and TargetScan [52, https://www.targetscan.org//] were used to identify target genes for miR-631 **(S1 Table)**.

Patient sample collection

This study used a total of 36 matched normal oral tissue and OSCC patient samples that were collected at the Kidwai Memorial Institute of Oncology (KMIO), Bangalore, from 13th July, 2018 to 14th November, 2018. The study was conducted with written informed consent

602 from the patients and approval from the ethics committee of the KMIO (approval
603 #KMIO/MEC/021/05.January.2018). It adhered to the principles of the Helsinki Declaration.
604 The samples, consisting of surgically resected tissues from oral cancerous lesions and adjacent
605 normal tissues (taken from the farthest margin of surgical resection), were preserved in
606 RNALater™ (Sigma-Aldrich, St. Louis, MO, USA) and stored at -80˚C until further use.
607 Tumors were staged according to the TNM (Tumor, Node, and Metastasis) classification of the
608 UICC (International Union against Cancer; https://www.uicc.org/). The summary of the patient
609 cohort is tabulated in **S3 Table**, and details of clinicopathological features for each patient
610 sample is mentioned in **S4 Table**.
611
612 **Total RNA extraction and qRT-PCR**
613 Total RNA from cell lines and tissues was isolated using the TRI Reagent™ (Sigma-
614 Aldrich, St. Louis, MO, USA). RNA was quantitated using a NanoDrop 1000
615 spectrophotometer (Thermo Fisher Scientific, Waltham, MA, USA). First-strand cDNA
616 synthesis was performed using 1–2 µg of total RNA and a Verso cDNA Synthesis Kit (Thermo
617 Fischer Scientific, Waltham, MA, USA). The expression of miR-631 was determined as
618 suggested by Sharbati-Tehrani [53], using specific primers **(S5 Table)**. The change in
619 expression of *RAB11A* was determined using qRT-PCR and transcript specific primers **(S5**
620 **Table)**.
621
622 ***In silico* identification of the putative *MIR631* promoter**
623 The putative promoter sequence for the *MIR631* gene was retrieved from the DBTSS
624 database [54; https://dbtss.hgc.jp/], and verified using promoter identifying algorithms such as
625 Promoter 2.0 [55; https://services.healthtech.dtu.dk/services/Promoter-2.0/] and Alggen Promo
626 [56; http://alggen.lsi.upc.es/].
627
628 **Plasmid constructs**
629 To overexpress miR-631 in cells, the pmiR-631 construct was generated in the
630 pcDNA3-EGFP vector, downstream to the CMV promoter. The promoter characterization of
631 *MIR631* was conducted using constructs where putative promoter fragment retrieved from the
632 DBTSS database was cloned upstream to the luciferase gene in the pGL3-Basic vector
633 (Promega, Madison, WI, USA) to generate pProm-MIR631. Overexpression of *RAB11A* was
634 carried out by cloning *RAB11A* ORF in the pcDNA3.1(+) vector to generate pRAB11A.

635 The direct binding of miR-631 to the *RAB11A* 3'UTR was confirmed by a dual-
636 luciferase reporter assay. For this experiment, two constructs namely p3'UTR-RAB11A-S and
637 p3'UTR-RAB11A-M were generated. The p3'UTR-RAB11A-S construct includes an intact 7-
638 mer target site for miR-631 binding in the 3'UTR of *RAB11A* and was cloned in the pMIR-
639 REPORT™ vector (Invitrogen, Waltham, MA, USA). Whereas, the p3'UTR-RAB11A-M
640 construct containing a mutated 3'UTR that lacks the miR-631 target site was generated by site-
641 directed mutagenesis, using a standard laboratory protocol [57]. As a positive control, the 3'
642 UTR of the *PTPRE* gene was also cloned in the pmiR-REPORT™ vector, and the construct
643 was named as p3'UTR-PTPRE-S.
644 To further examine the ability of miR-631 to downregulate RAB11A protein levels via
645 direct binding to the *RAB11A* 3'UTR, two additional constructs were generated: pRAB11A-
646 UTR-S and pRAB11A-UTR-M. To this end, the *RAB11A* ORF that was cloned in the
647 pcDNA3.1(+) vector (i.e., pRAB11A) was linked to either the *RAB11A* 3'UTR in a sense
648 orientation (pRAB11A-UTR-S) or the mutated 3'UTR lacking the miR-631 binding site
649 (pRAB11A-UTR-M). All the constructs used in the study were validated by restriction enzyme
650 digestion and Sanger sequencing on a 3730xl DNA Analyzer (Thermo Fisher Scientific,
651 Waltham, MA, USA). Details of the primers used in generating the above constructs are given
652 in **S6 Table**.
653
654 **Cell culture, transient transfection, and reporter assays**
655 Cells were maintained in Dulbecco's modified eagle medium (DMEM), supplemented
656 with 10% (v/v) fetal bovine serum (FBS) and 1X antibiotic-antimycotic solution [DMEM and
657 1X antibiotic-antimycotic solution purchased from Sigma-Aldrich, St. Louis, MO, USA; FBS
658 purchased from Thermo Fisher Scientific, Waltham, MA, USA] in a humidified incubator with
659 5% CO_2 at 37˚C.
660 SCC131 or SCC084 cells were seeded at a density of 2×10^6 cells/well in a 6-well plate
661 and transiently transfected with an appropriate construct or co-transfected with a combination
662 of constructs, using the Lipofectamine™ 2000 transfection reagent (Thermo Fisher Scientific,
663 Waltham, MA, USA), following the manufacturer's protocol. Post 48 hr of transfection, total
664 RNA and protein were isolated from cells as described below.
665 The direct interaction between the 3'UTR of the target gene and miR-631 as well as the
666 promoter activity of the constructs were determined, using a dual-luciferase reporter assay kit
667 (Promega, Madison, WI, USA). For this purpose, 5×10^4 cells/well were transfected with
668 different constructs as mentioned above. The assay was carried out after 48 hr of transfection

669 in SCC131 cells, using the dual-luciferase reporter assay and the VICTOR X multilabel plate
670 reader (PerkinElmer, Waltham, MA, USA). The transfection efficiency in the dual-luciferase
671 reporter assay was normalized by co-transfecting with the pRL-TK control vector [10, 13].
672 For the Wnt signaling analysis, the TOPflash reporter plasmid (Sigma-Aldrich, St.
673 Louis, MO, USA) was transiently transfected along with other overexpression construct(s) for
674 in SCC131 cells (5×10^4 cells/well) as described by Choi et al. [40]. The transfection efficiency
675 in the dual-luciferase reporter assay was normalized by co-transfecting with the pRL-TK
676 control vector and the TOPflash control vector (Sigma-Aldrich, St. Louis, MO, USA) [10, 13].
677
678 **5-Azacytidine treatment of cells**
679 SCC131 cells were grown for 24 hr and treated with 5-Azacytidine (Sigma-Aldrich, St.
680 Louis, MO, USA) at a final concentration of 5 μM or the vehicle control DMSO (Sigma-
681 Aldrich, St. Louis, MO, USA) separately for 5 days. Total RNA, protein, and genomic DNA
682 were isolated from 5-Azacytidine- and DMSO-treated cells for further studies [10].
683
684 **Methylation analysis of the *MIR631* promoter**
685 Genomic DNA isolated from 5-Azacytidine- and DMSO-treated cells were treated with
686 3.25 M sodium bisulphite (Sigma-Aldrich, St. Louis, MO, USA) to convert non-methylated
687 cytosines to uracil, according to Frommer et al. [58]. The converted DNA was subsequently
688 used in PCR, using the following primers specifically designed for bisulfite-treated DNA:
689 forward primer (5'- AGATCGTTAAGTAGGTAAGGGGTG-3') and reverse primer (5'-
690 CACTCACAAAATAACCTCCTAAACC-3'). The 212bp long amplified fragments were
691 cloned in a TA-cloning vector pTZ57R (Fermentas, Waltham, MA, USA) and 10 clones from
692 each treatment were sequenced on a 3730xl DNA Analyzer to identify methylated and
693 unmethylated cytosines.
694
695 **Western blot hybridization**
696 Lysates from cells were made using the CelLytic™ M Cell Lysis Reagent (Sigma-
697 Aldrich, St. Louis, MO, USA), while the CelLytic ™ MT Mammalian Tissue Lysis Reagent
698 (Sigma- Aldrich, St. Louis, MO, USA) was used to prepare lysates from oral tissue samples.
699 After resolving the proteins in the lysates in a SDS-PAGE gel (Sodium dodecyl sulfate-
700 Polyacrylamide gel electrophoresis), they were transferred to a PVDF membrane (Pall Corp.,
701 Port Washington, NY, USA), using a semi-dry transfer apparatus. The blotting membrane was

702 then kept for blocking in 5% skimmed milk (Nestle, Gurgaon, India) in 1X PBST (Phosphate
703 buffered saline tween 20).
704 After the blocking, three PBST washes were given, and the membrane was incubated
705 with corresponding primary and secondary antibodies. An anti-RAB11A antibody (1:10,000
706 dilution, cat#ab128913) was purchased from Abcam (Cambridge, MA, USA). The anti-mouse
707 β-actin (1:10,000 dilution, cat# A5441) purchased from Sigma-Aldrich (St. Louis, MO, USA)
708 was used as a loading control. The anti-rabbit HRP-conjugated secondary antibody (1.5:5,000
709 dilution, cat# HP03) and anti-mouse HRP-conjugated secondary antibody (1:5,000 dilution,
710 cat# HP06) were purchased from Bangalore Genei (Bangalore, India).
711
712 **Cell proliferation assays**
713 The rate of proliferation of SCC131 and SCC084 cells transfected with an appropriate
714 construct or co-transfected with a combination of constructs was assessed by the trypan blue
715 dye exclusion assay as described by [59]. Cell proliferation was also determined using a
716 BrdU cell proliferation assay kit (Sigma-Aldrich, Germany), as described in Sarkar et al.
717 [10].
718 **Apoptosis assay**
719 The CaspGLOW Fluorescein Active Caspase-3 Staining kit (BioVision, Milpitas, CA,
720 USA) was used to quantify the apoptosis of cells transfected with the appropriate constructs,
721 according to the manufacturer's instructions and as described by Rather et al. [13].
722
723 **Soft agar colony-forming assay**
724 Tumor cells can overcome anoikis to proliferate and form colonies in suspension within
725 a semi-solid medium such as soft agar [60]. The anchorage-independent growth of cells co-
726 transfected with a combination of constructs was analyzed by the soft agar colony-forming
727 assay in 35 mm tissue culture dishes, following a standard laboratory protocol [10].
728
729 ***In vivo* assay for tumor growth**
730 The effect of a synthetic miR-631 mimic on OSCC tumor growth was assayed in 6
731 weeks old female NU/J athymic nude mice. Briefly, 2×10^6 SCC131 cells/well were seeded in
732 two 6-well plates. Following overnight incubation of the cells in a CO_2 incubator, each of the
733 six wells of a plate was transfected with 400 nM of a synthetic miR-631 mimic. The same
734 procedure was repeated for the mimic control. Post 24 hr of transfection, cells from each plate

735 were harvested and pooled together. Further, 3×10^6 transfected cells from each pooled group
736 of cells were suspended in 200 µL of 1:1 dilution of DPBS and matrigel
737 [Corning Matrigel Growth Factor Reduced Basement Membrane Matrix, LDEV-free, cat #
738 354230, NY, USA] in a 1.5 mL tube (6 tubes/pooled group). Cell suspension from each tube
739 was then subcutaneously injected in each posterior flank of each of the three mice. Tumors
740 were allowed to grow in animals, and tumor volumes were measured using a Vernier calliper
741 every alternate day till the termination of the experiment.
742 Tumor volumes were calculated using the following formula: $V = L\times W^2\times0.5$, where L
743 and W represent the length and width of the tumor respectively [10, 14, 15]. The animals were
744 photographed, and the tumor xenografts were harvested at the end of the study. Harvested
745 xenografts were also photographed and weighed. This study was carried out in accordance with
746 the recommendations in the Guide for the Care and Use of Laboratory Animals of the National
747 Institutes of Health and ARRIVE guidelines (https://arriveguidelines.org/). The animal
748 experimental protocol was approved by the Institutional Animal Ethics Committee, IISc,
749 Bangalore (approval certificate# CAF/Ethics/936/2023). All mice were maintained on a 12:12
750 hr light/dark cycle in proper cages with sufficient food and water. At the end of the study,
751 animals were euthanized under sterile conditions using isofluracil (Sigma-Aldrich, Germany)
752 followed by cervical dislocation by trained personnel. The miRIDIAN miRNA hsa-miR-631-
753 Mimic (cat#C-300957-01-0020) and miRIDIAN miRNA Mimic Negative Control #1 (cat#CN-
754 001000-01-20) were purchased from Dharmacon (Lafayette, CO, USA).
755
756 **Statistical analysis**
757 A two-tailed student's t-test was performed using the GraphPad PRISM8 software
758 (GraphPad Software Inc., San Diego) to analyze the statistical significance of the difference
759 between two data sets, with Welch's correction wherever required. Differences with P-value
760 0.05 (*), P-value <0.01 (**), P-value <0.001 (***), and P-value <0.0001 (****) were
761 considered statistically significant, whereas P-value >0.05 was considered as statistically non-
762 significant (ns).
763
764 **Acknowledgements**
765 We are grateful to the patients for providing the normal and tumor oral samples.
766
767

768

769

770 **Figure legends**

771

772 **Fig 1. Characterization of the *MIR631* promoter and deciphering the mechanism of miR-**
773 **631 upregulation in SCC131 cells. (**A) The dual-luciferase reporter assay shows an increased
774 luciferase activity for the putative promoter fragment cloned in pProm-MIR631. pGL3-Basic
775 is a promoter less vector, whereas pGL3-Control harbors the SV40 promoter and was used a
776 positive control. Each bar in the dual-luciferase reporter assay is an average of three technical
777 replicates. (B) Schematic representation of the *MIR631* promoter with a 212 bp long CpG
778 island harboring 14 CpG sites. Pre-miR-631 represents the location of the precursor sequence
779 of miR-631. (C) Schematic representation of the methylation pattern of the CpG island. Filled
780 circles represent methylated CpG sites, whereas empty circles represent non-methylated CpG
781 sites. Each line represents a single TA clone. *Abbreviations:* RLU, Relative light unit; Meth
782 Fp, Methylation specific forward primer; and, Meth Rp, Methylation specific reverse primer.

783

784 **Fig 2. Identification of *RAB11A* as a gene target for miR-631.** (A) Overexpression of miR-
785 631 using the pmiR-631 construct in SCC131 cells leads to reduced RAB11A transcript and
786 protein levels. (B) The dose-dependent regulation of RAB11A transcript and protein levels in
787 SCC131 cells with increasing quantities of pmiR-631. (C) Reduced levels of RAB11A
788 transcript and protein following the 5-Azacytidine treatment of SCC131 cells with the
789 concomitant increase in miR-631 levels. Each bar for qRT-PCR is an average of two technical
790 replicates.

791

792 **Fig 3. Confirmation of a direct interaction between miR-631 and the 3'UTR of *RAB11A***
793 (A) Conservation of the putative TS in the 3'UTR of *RAB11A* across different species for the
794 SR of miR-631. (B) Schematic representation of the constructs used in the dual-luciferase
795 reporter assay. The X indicates abrogated TS or SR in a construct. (C) The dual-luciferase
796 reporter assay in SCC131 cells co-transfected with different constructs. Note, reduced RLU in
797 cells co-transfected with p3'UTR-RAB11A-S and pmiR-631 compared to those co-transfected
798 with the vector control and pmiR-631. Each bar is an average of three technical replicates.
799 *Abbreviations:* TS, Target Site; and SR, Seed Region.

800

801 **Fig 4. Regulation of *RAB11A* by miR-631 is mediated by its 3'UTR and the impact of this**
802 **regulation on proliferation of SCC131 cells. (**A) The RAB11A protein levels are dependent
803 on the presence or absence of a functional TS in its 3'UTR for miR-631. Schematic diagrams
804 of different *RAB11A* constructs are shown above the Western blots. (B) The negative regulation
805 of cell proliferation by miR-631, in part, via targeting the 3'UTR of *RAB11A*, using the trypan
806 blue dye exclusion assay. (B) The negative regulation of cell proliferation by miR-631, in part,
807 via targeting the 3'UTR of *RAB11A*, using the BrdU incorporation assay. Each datapoint is an
808 average of three values.

809 **Fig. 5. Regulation of anchorage-independent growth and apoptosis by miR-631, in part,**
810 **via targeting the 3'UTR of *RAB11A* in SCC131 cells.** (A) The negative regulation of
811 anchorage-independent growth by miR-631, in part, via targeting the 3'UTR of *RAB11A.*
812 Representative microphotographs of the colonies for SCC131 cells co-transfected with pmiR-
813 631 and different *RAB11A* overexpression constructs or vector control from the soft agar
814 colony-forming assay are shown on the right. The bar represents 100 nm. (B) The positive
815 regulation of apoptosis by miR-631, in part, via targeting the 3'UTR of *RAB11A.* Each
816 datapoint is an average of three values.

817 **Fig 6. The effect of a synthetic miR-631 mimic on SCC131 cells-derived xenografts in**
818 **nude mice. (**A) Top panel: Photographs of nude mice showing tumor growth on Day 23 of
819 injection of cells pre-treated with a synthetic miR-631 Mimic (MM) or Mimic Control (MC).
820 Bottom Panel: Excised xenografts from each mouse on Day 23. Xenografts are circled by red
821 dash lines and labelled Left (L) and Right (R) according to the flanks they were excised from.
822 Note, there was no tumor formation in nude mouse, MC3. (B) Effect of a synthetic miR-631
823 mimic on tumor volumes during a time course of 7-23 days, and overall tumor weight of
824 xenografts on Day 23. (C) qRT-PCR and Western blot analyzes of excised xenografts from the
825 miR-631 mimic and the mimic control groups. Note, increased levels of miR-631 (Top panel)
826 are correlated with reduced levels of RAB11A (Bottom panel) in xenografts with the miR-631
827 mimic as compared to those with the mimic control.
828
829 **Supporting information**
830
831 **S1 Fig. Validation of miR-631 upregulation post 5-Azacytidine treatment.**
832

833 **S2 Fig. Effect of miR-631 on OSCC cell proliferation.**

834

835 **S3 Fig. Diagrammatic representation of the genomic location of miR-631 and pre-miR-**
836 **631 stem-loop.**

837

838 **S4 Fig. Diagrammatic representation of the *MIR631* promoter sequence.**

839

840 **S5 Fig. Regulation of predicted target genes by miR-631.**

841

842 **S6 Fig. The effect of *RAB11A* on cell proliferation.**

843

844 **S7 Fig. Expression levels of miR-631 and *RAB11A* in different cancer cell lines.**

845

846 **S8 Fig. Expression levels of miR-631 and *RAB11A* in 36 matched normal oral tissue and**
847 **OSCC patient samples.**

848

849 **S9 Fig. The negative regulation of RAB11A by miR-631 is mediated by its 3'UTR and the**
850 **impact of this regulation on proliferation of SCC084 cells.**

851

852 **S10 Fig. Regulation of anchorage-independent growth and apoptosis by miR-631, in part,**
853 **via targeting the 3'UTR of *RAB11A* in SCC084 cells.**

854

855 **S11 Fig. RAB11A enhances Wnt signaling, while miR-631 negatively regulates it in**
856 **SCC131 and SCC084 cells.**

857

858 **S12 Fig. miR-631 negatively regulates Wnt signaling, in part, by targeting the 3'UTR of**
859 ***RAB11A* in SCC131 and SCC084 cells.**

860

861 **S13 Fig. Optimization of the dosage for a synthetic miR-631 mimic in SCC131 cells.**

862

863

864 **S1 Table. Predicted target genes for miR-631.**

865

866 **S2 Table. Bioinformatics analysis of selected target genes.**

867

868 **S3 Table. Summary of the patient samples used in the study.**

869

870 **S4 Table. Clinicopathological parameters of the patients used in the study.**

871

872 **S5 Table. Details of primers used in qRT-PCR.**

873

874 **S6 Table. Details of plasmid constructs used in the study.**

875

876 **S1 Raw images**.

877

878 **References**

879

880 1. Badwelan M, Muaddi H, Ahmed A, Lee KT, Tran SD. Oral Squamous Cell Carcinoma and
881 Concomitant Primary Tumors, What Do We Know? A Review of the Literature. Current
882 Oncology. 2023 Mar 27;30(4):3721–34. doi:10.3390/curroncol30040283.

883

884 2. Tan Y, Wang Z, Xu M, Li B, Huang Z, Qin S, et al. Oral squamous cell carcinomas: state of
885 the field and emerging directions. Int J Oral Sci. 2023;15(1):44. doi: 10.1038/s41368-023-
886 00249-w.

887

888 3. Jethwa AR, Khariwala SS. Tobacco-related carcinogenesis in head and neck cancer. Cancer
889 Metastasis Rev. 2017 Sep; 36(3):411–23. doi: 10.1007/s10555-017-9689-6.

890

891 4. Dunn LA, Fury MG, Sherman EJ, Ho AA, Katabi N, Haque SS, et al. Phase I study of
892 induction chemotherapy with afatinib, ribavirin, and weekly carboplatin and paclitaxel for
893 stage IVA/IVB human papillomavirus-associated oropharyngeal squamous cell cancer. Head
894 & Neck. 2018 Feb; 40(2):233–41. doi: 10.1002/hed.24938.

895

896 5. Donaldson MS. Nutrition and cancer: A review of the evidence for an anti-cancer diet. Nutr
897 J. 2004 Oct 20; 3(1):19. doi: 10.1186/1475-2891-3-19.

898

899 6. Dharmawardana N, Goddard T, Woods C, Watson DI, Ooi EH, Yazbeck R. Development
900 of a non-invasive exhaled breath test for the diagnosis of head and neck cancer. Br J Cancer.
901 2020 Dec 8; 123(12):1775–81. doi: 10.1038/s41416-020-01051-9.

902

903 7. Das B, Nagpal N. Understanding the biology of oral cancer. 8. RA258-67. In Medical
904 science monitor: international medical journal of experimental and clinical research. 2002.
905 PMID: 12444391.

906

907 8. Sarkar N, Kumar A. microRNAs: New-Age Panacea in Cancer Therapeutics. *Indian J Surg*
908 *Oncol*. 2021;12(Suppl 1):52-56. doi: 10.1007/s13193-020-01110-w.

909

910 9. O'Brien J, Hayder H, Zayed Y, Peng C. Overview of microRNA biogenesis, mechanisms of
911 actions, and circulation. Front Endocrinol. 2018 Aug 3; 9:402. doi: 10.3389/fendo.2018.00402.

10. Sarkar N, Mishra R, Gopal C, Kumar A. miR-617 interacts with the promoter of *DDX27* and positively regulates its expression: implications for cancer therapeutics. Front Oncol. 2024 Jun 13; 14:1411539. doi: 10.3389/fonc.2024.1411539.

11. Sarkar N, Kumar A. Paradigm shift: microRNAs interact with target gene promoters to cause transcriptional gene activation or silencing. Experimental Cell Research. 2025 Jan ;444(2):114372. doi: 10.1016/j.yexcr.2024.114372.

12. Hanna J, Hossain GS, Kocerha J. The potential for microRNA therapeutics and clinical research. Front Genet. 2019 May 16; 10:478. doi: 10.3389/fgene.2019.00478.

13. Rather MI, Nagashri MN, Swamy SS, Gopinath KS, Kumar A. Oncogenic microRNA-155 down-regulates tumor suppressor *CDC73* and promotes oral squamous cell carcinoma cell proliferation. Journal of Biological Chemistry. 2013 Jan; 288(1):608–18. doi: 10.1074/jbc.M112.425736.

14. More DA, Singh N, Mishra R, Muralidharan HP, Gopinath KS, Gopal C, et al. Intronic miR-6741-3p targets the oncogene SRSF3: Implications for oral squamous cell carcinoma pathogenesis. PLoS ONE. 2024 May 23; 19(5): e0296565. doi: 10.1371/journal.pone.0296565.

15. Kaushik P, Mishra R, Gopal C, Kumar A. miR-198 targets TOPORS: implications for oral squamous cell carcinoma pathogenesis. Front Oncol. 2024 Dec 4; 14:1485802. doi: 10.3389/fonc.2024.1485802.

16. Peng Y, Croce CM. The role of microRNAs in human cancer. Sig Transduct Target Ther. 2016 Jan 28; 1(1):15004. doi: 10.1038/sigtrans.2015.4.

940 17. Gasche JA, Goel A. Epigenetic mechanisms in oral carcinogenesis. Future Oncol. 2012
941 Nov;8(11):1407–25. doi: 10.2217/fon.12.138.
942
943 18. D'Souza W, Kumar A. microRNAs in oral cancer: Moving from bench to bed as next
944 generation medicine. *Oral Oncol*. 2020; 111:104916. doi:
945 10.1016/j.oraloncology.2020.104916.
946
947 19. Jithesh PV, Risk JM, Schache AG, Dhanda J, Lane B, Liloglou T, et al. The epigenetic
948 landscape of oral squamous cell carcinoma. Br J Cancer. 2013 Feb; 108(2):370–9. doi:
949 10.1038/bjc.2012.568.
950
951 20. Christman JK. 5-Azacytidine and 5-aza-2′-deoxycytidine as inhibitors of DNA
952 methylation: mechanistic studies and their implications for cancer therapy. Oncogene. 2002
953 Aug 12; 21(35):5483–95. doi: 10.1038/sj.onc.1205699.
954
955 21. Purwaningsih NMS, Khor GH, Nik Mohd Rosdy NMM, Abdul Rahman EO. Wnt pathway
956 in oral cancer: A review update. *Saudi Dent J*. 2021;33(8):813-818. doi:
957 10.1016/j.sdentj.2021.08.002.
958
959 22. Fu D, Liu B, Zang LE, Jiang H. MiR-631/*ZAP70*: A novel axis in the migration and
960 invasion of prostate cancer cells. Biochemical and Biophysical Research Communications.
961 2016 Jan; 469(3):345–51. doi: 10.1016/j.bbrc.2015.11.093.
962
963 23. Chen B, Liao Z, Qi Y, Zhang H, Su C, Liang H, et al. miR-631 inhibits intrahepatic
964 metastasis of hepatocellular carcinoma by targeting *PTPRE*. Front Oncol. 2020 Dec 4;
965 10:565266. doi: 10.3389/fonc.2020.565266.
966

24. Xi H, Li L, Du J, An R, Fan R, Lu J, et al. hsa-miR-631 resensitizes bortezomib-resistant multiple myeloma cell lines by inhibiting UbcH10. Oncology Reports. 2017 Jan; 37(2):961–8. doi: 10.3892/or.2016.5318.

25. Chen JC, Shih HC, Lin CY, Guo JH, Huang C, Huang HC, et al. MicroRNA-631 resensitizes doxorubicin-resistant chondrosarcoma cells by targeting Apelin. Int J Mol Sci. 2023 Jan 3;24(1):839. doi: 10.3390/ijms24010839.

26. Lv H, Yu J, Zhang H, Qian X, Wang Q, Lu B, et al. MicroRNA-631 deriving from bone marrow mesenchymal stem cell exosomes facilitates the malignant behavior of non-small cell lung cancer via modulating the E2F family of transcription factor 2/phosphatidylinositol 3-kinase/Akt signaling pathway. Bioengineered. 2022 Apr 1;13(4):8382–95. doi: 10.1080/21655979.2022.2036891.

27. Lee HA, Ahn EH, Jang HG, Kim JO, Kim JH, Lee YB, et al. Association Between miR-605 A>G, miR-608 G>C, miR-631 I>D, miR-938 C>T, and miR-1302-3 C>T polymorphisms and risk of recurrent implantation failure. Reprod Sci. 2019 Apr ;26(4):469–75. doi: 10.1177/1933719118773413.

28. Chen SF, Liu Z, Chaurasiya S, Dellinger TH, Lu J, Wu X, et al. Identification of core aberrantly expressed microRNAs in serous ovarian carcinoma. Oncotarget.; 2018. doi: 10.18632/oncotarget.24942.

29. Shaanbanpour Aghamaleki F, Mollashahi B, Aghamohammadi N, Rostami N, Mazloumi Z, Mirzaei H, et al. Bioinformatics analysis of key genes and pathways for medulloblastoma as a therapeutic target. Asian Pac J Cancer Prev. 2019 Jan 1; 20(1):221–7. doi: 10.31557/APJCP.2019.20.1.221.

995 30. Dong Q, Fu L, Zhao Y, Du Y, Li Q, Qiu X, et al. Rab11a promotes proliferation and
996 invasion through regulation of YAP in non-small cell lung cancer. Oncotarget. 2017 Apr
997 25;8(17):27800–11. doi: 10.18632/oncotarget.15359.

998

999 31. Du J, Fu L, Hao J, Lin X, Dong Q. Rab11a is overexpressed in gastric cancer and regulates
1000 FAK/AKT signaling. J Oncol. 2020; 3494396. doi: 10.1155/2020/3494396.

1001

1002 32. Wang B, Yang Z, Wang H, Cao Z, Zhao zY, Gong C, et al. MicroRNA-320a inhibits
1003 proliferation and invasion of breast cancer cells by targeting RAB11A. Am J Cancer Res.
1004 2015;5(9):2719–29. PMID: 26609479

1005

1006 33. Li W, Li G, Fan Z, Liu T. Tumor-suppressive microRNA-452 inhibits migration and
1007 invasion of breast cancer cells by directly targeting RAB11A. Oncology Letters. 2017 Aug;
1008 14(2):2559–65. doi: 10.3892/ol.2017.6426.

1009

1010 34. Wang Y, Li N, Zhao J, Dai C. MiR-193a-5p serves as an inhibitor in ovarian cancer cells
1011 through RAB11A. Reproductive Toxicology. 2022 Jun 1; 110:105–12. doi:
1012 10.1016/j.reprotox.2022.04.003.

1013

1014 35. Yoshida K, Htike K, Eguchi T, Kawai H, Eain HS, Tran MT, et al. Rab11 suppresses head
1015 and neck carcinoma by regulating EGFR and EpCAM exosome secretion. Journal of Oral
1016 Biosciences.2024 Mar; 66(1):205–16. doi: 10.1016/j.job.2023.11.007.

1017

1018 36. Michor F, Polyak K. The origins and implications of intratumor heterogeneity. *Cancer Prev*
1019 *Res (Phila)*. 2010;3(11):1361-1364. doi: 10.1158/1940-6207.

1020

1021 37. Ghosh RD, Pattatheyil A, Roychoudhury S. Functional Landscape of Dysregulated
1022 MicroRNAs in Oral Squamous Cell Carcinoma: Clinical Implications. *Front Oncol*. 2020;
1023 10:619. Published 2020 May 12. doi: 10.3389/fonc.2020.00619.

1024

1025 38. Mallela K, Shivananda S, Gopinath KS, Kumar A. Oncogenic role of miR-130a in oral
1026 squamous cell carcinoma. Sci Rep. 2021 Apr 8;11(1):7787. doi: 10.1038/s41598-021-87388-
1027 4.

1028

1029 39. Yu L, Li X, Li H, Chen H, Liu H. Rab11a sustains GSK3β/Wnt/β-catenin signaling to
1030 enhance cancer progression in pancreatic cancer. Tumour Biol. 2016 Oct;37(10):13821–9. doi:
1031 10.1007/s13277-016-5172-1.

1032

1033 40. Choi JY, Lai JK, Xiong ZM, Ren M, Moorer MC, Stains JP, et al. Diminished canonical β-
1034 catenin signaling during osteoblast differentiation contributes to osteopenia in progeria. J Bone
1035 Miner Res. 2018 Nov;33(11):2059–70. doi: 10.1002/jbmr.3549.

1036

1037 41. Zhao D, Wang B, Chen H. RAB11A mediates the proliferation and motility of esophageal
1038 cancer cells via WNT signaling pathway. *Acta Biochim Pol*. 2020;67(4):531-538. doi:
1039 10.18388/abp.2020_5392.

1040

1041 42. Prgomet Z, Axelsson L, Lindberg P, Andersson T. Migration and invasion of oral squamous
1042 carcinoma cells is promoted by WNT5A, a regulator of cancer progression. *J Oral Pathol Med*.
1043 2015;44(10):776-784. doi: 10.1111/jop.12292.

1044

1045 43. Li L, Liu HC, Wang C, et al. Overexpression of β-Catenin Induces Cisplatin Resistance in
1046 Oral Squamous Cell Carcinoma. *Biomed Res Int*. 2016; 5378567. doi: 10.1155/2016/5378567.

1047

1048

1049 44. Garreau M, Weidner J, Hamilton R, Kolosionek E, Toki N, Stavenhagen K, et al. Chemical
1050 modification patterns for microRNA therapeutic mimics: a structure-activity relationship
1051 (SAR) case-study on miR-200c. Nucleic Acids Research. 2024 Apr 12;52(6):2792–807. doi:
1052 10.1093/nar/gkae141.

1053

1054 45. Trang P, Wiggins JF, Daige CL, Cho C, Omotola M, Brown D, et al. Systemic Delivery of
1055 Tumor Suppressor microRNA Mimics Using a Neutral Lipid Emulsion Inhibits Lung Tumors
1056 in Mice. Molecular Therapy. 2011 Jun;19(6):1116–22. doi: 10.1038/mt.2011.48.

1057

1058 46. Di Martino MT, Leone E, Amodio N, et al. Synthetic miR-34a mimics as a novel
1059 therapeutic agent for multiple myeloma: in vitro and in vivo evidence. *Clin Cancer Res*.
1060 2012;18(22):6260-6270. doi: 10.1158/1078-0432.

1061

1062 47. White JS, Weissfeld JL, Ragin CCR, Rossie KM, Martin CL, Shuster M, et al. The
1063 influence of clinical and demographic risk factors on the establishment of head and neck
1064 squamous cell carcinoma cell lines. Oral Oncol. 2007 Aug;43(7):701–12. doi:
1065 10.1016/j.oraloncology.2006.09.001.

1066

1067 48. Chen Y, Wang X. miRDB: an online database for prediction of functional microRNA
1068 targets. Nucleic Acids Res. 2020 Jan 8;48(D1): D127–31. doi: 10.1093/nar/gkz757.

1069

1070 49. Paraskevopoulou MD, Georgakilas G, Kostoulas N, Vlachos IS, Vergoulis T, Reczko M,
1071 et al. DIANA-microT web server v5.0: service integration into miRNA functional analysis
1072 workflows. Nucleic Acids Res. 2013 Jul;41: W169-173. doi: 10.1093/nar/gkt393.

1073

1074 50. Sticht C, De La Torre C, Parveen A, Gretz N. miRWalk: An online resource for prediction
1075 of microRNA binding sites. PLoS One.; 2018. doi: 10.1371/journal.pone.0206239.

1076

1077 51. Quillet C, Saad, G, Ferry, Y, Anouar, N, Vergne, T, Lecroq, et al. Improving bioinformatics
1078 prediction of microRNA targets by ranks aggregation. Frontiers in Genetics; 2020. doi:
1079 10.3389/fgene.2019.01330.

1080

1081 52. McGeary SE, Lin KS, Shi CY, et al. The biochemical basis of microRNA targeting
1082 efficacy. *Science*. 2019;366(6472):eaav1741. doi: 10.1126/science.aav1741.

1083

1084 53. Sharbati-Tehrani S, Kutz-Lohroff B, Bergbauer R, Scholven J, Einspanier R. miR-Q: a
1085 novel quantitative RT-PCR approach for the expression profiling of small RNA molecules such
1086 as miRs in a complex sample. BMC Mol Biol. 2008 Apr 10; 9:34. doi: 10.1186/1471-2199-9-
1087 34.

1088

1089 54. Suzuki A, Kawano S, Mitsuyama T, Suyama M, Kanai Y, Shirahige K, et al.
1090 DBTSS/DBKERO for integrated analysis of transcriptional regulation. Nucleic Acids Res.
1091 2018 Jan 4;46(D1): D229–38. doi: 10.1093/nar/gkx1001.

1092

1093 55. Steen Knudsen. Promoter 2.0: for the recognition of PolII promoter sequences.
1094 Bioinformatics 15; 1999. doi: 10.1093/bioinformatics/15.5.356.

1095

1096 56. Farré D, Roset R, Huerta M, Adsuara JE, Roselló L, Albà MM, et al. Identification of
1097 patterns in biological sequences at the ALGGEN server: PROMO and MALGEN. Nucleic
1098 Acids Res. 2003 Jul 1;31(13):3651–3. doi: 10.1093/nar/gkg605.

1099

1100 57. Ho SN, Hunt HD, Horton RM, Pullen JK, Pease LR. Site-directed mutagenesis by overlap
1101 extension using the polymerase chain reaction. *Gene*. 1989;77(1):51-59. doi: 10.1016/0378-
1102 1119(89)90358-2.

1103

1104 58. Frommer M, McDonald LE, Millar DS, Collis CM, Watt F, Grigg GW, et al. A genomic
1105 sequencing protocol that yields a positive display of 5-methylcytosine residues in individual
1106 DNA strands. Proc Natl Acad Sci U S A. 1992 Mar 1;89(5):1827–31. doi:
1107 10.1073/pnas.89.5.1827.

1108

1109 59. Karimi L, Zeinali T, Hosseinahli N, Mansoori B, Mohammadi A, Yousefi M, et al. miRNA-
1110 143 replacement therapy harnesses the proliferation and migration of colorectal cancer cells in
1111 vitro. J Cell Physiol. 2019 Nov; 234(11):21359–68. doi: 10.1002/jcp.28745.

1112

1113 60. Horibata S, Vo TV, Subramanian V, Thompson PR, Coonrod SA. Utilization of the soft
1114 agar colony formation assay to identify inhibitors of tumorigenicity in breast cancer cells. J
1115 Vis Exp. 2015 May 20;(99): e52727. doi: 10.3791/52727.

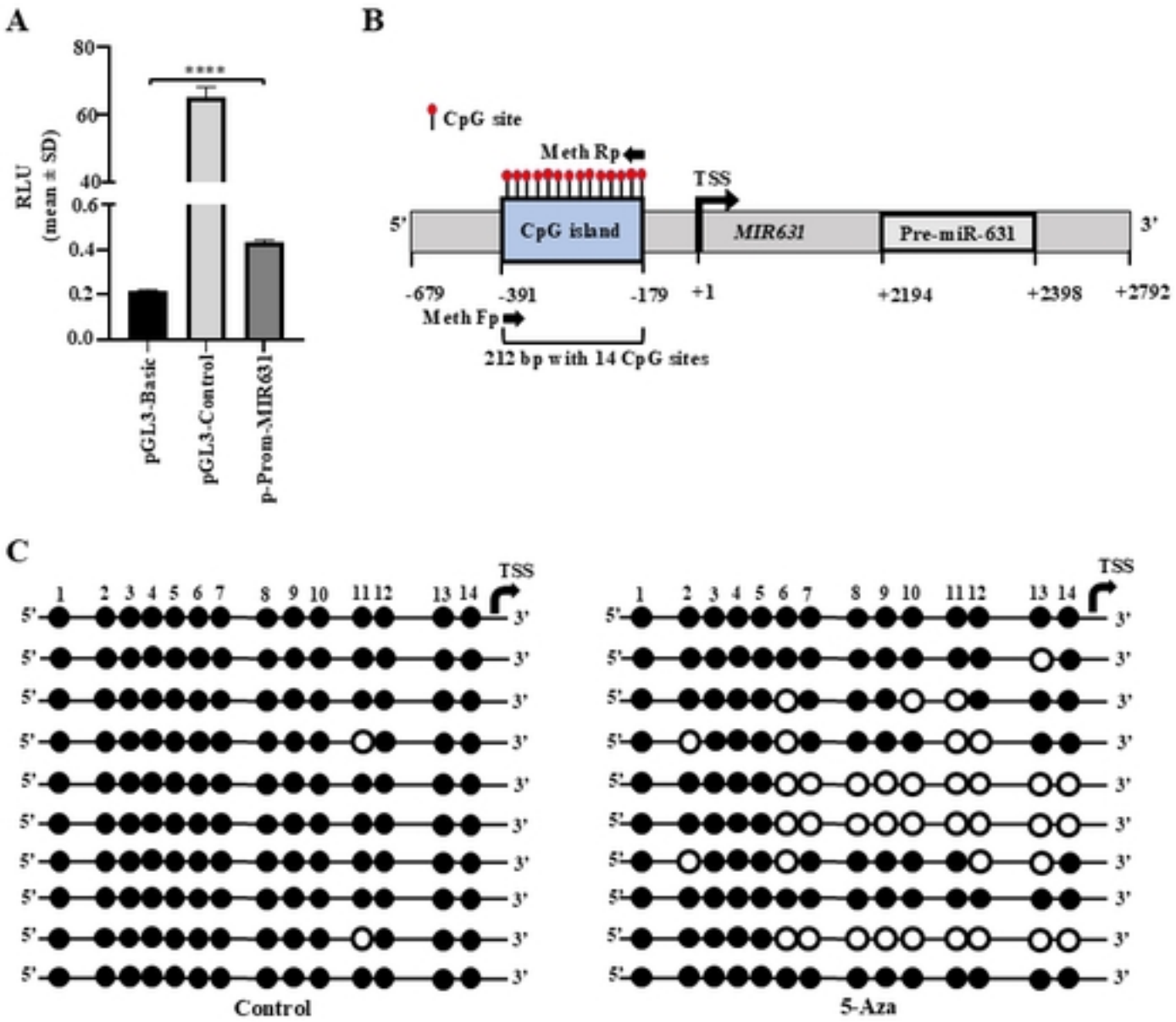
A
RLU
(mean ± SD)
80
60
40
0.6
0.4
0.2
0.0
****
pGL3-Basic
pGL3-Control
p-Prom-MIR631
B
CpG site
Meth Rp
TSS
5'
CpG island
MIR631
Pre-miR-631
3'
-679
-391
-179
+1
+2194
+2398
+2792
Meth Fp
212 bp with 14 CpG sites
C
TSS
1 2 3 4 5 6 7 8 9 10 11 12 13 14
Control
5-Aza

Fig 1

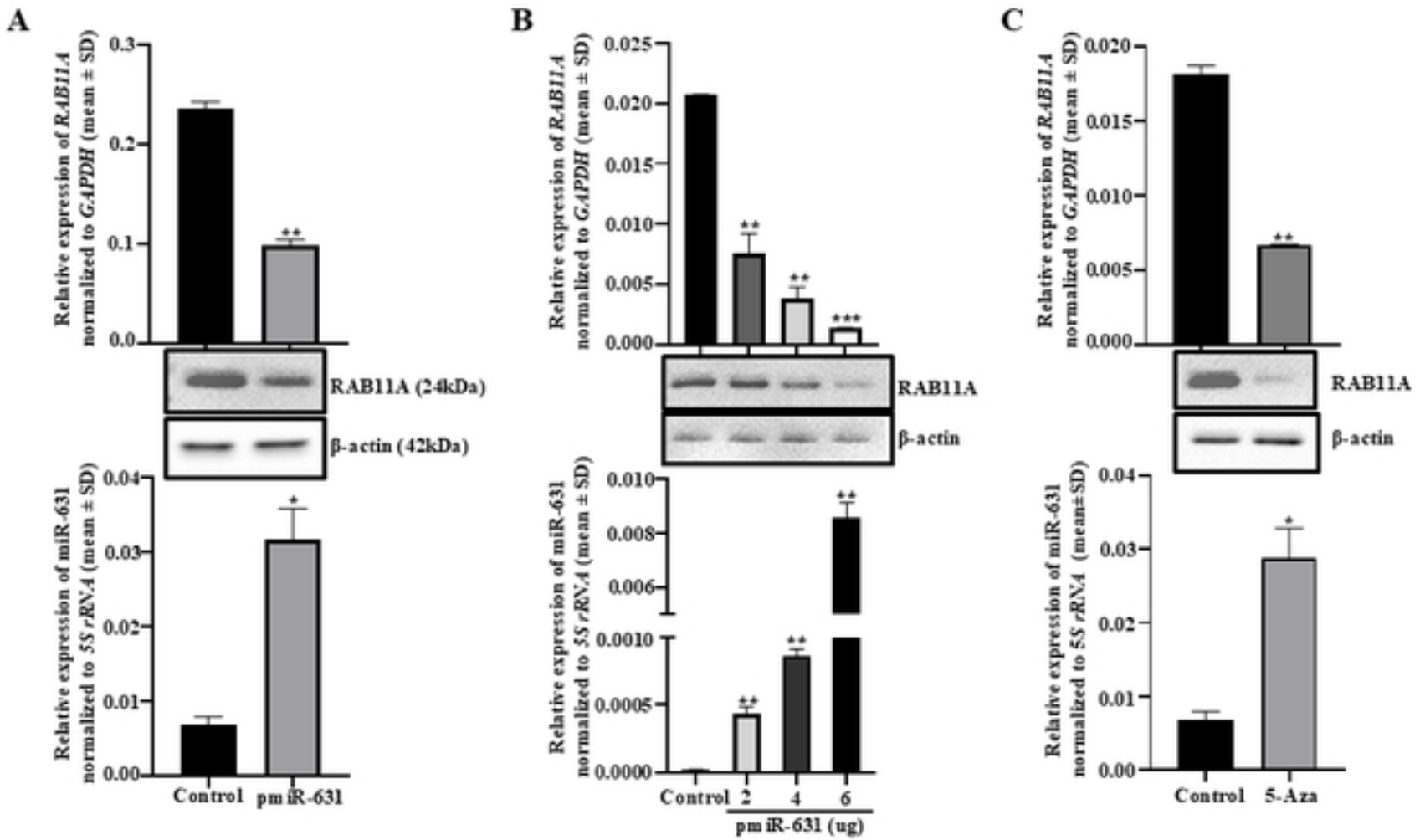
A
Relative expression of RAB11A normalized to GAPDH (mean ± SD)
0.3
0.2
0.1
0.0
**
RAB11A (24kDa)
β-actin (42kDa)
Relative expression of miR-631 normalized to 5S rRNA (mean ± SD)
0.04
0.03
0.02
0.01
0.00
*
Control
pmiR-631
B
Relative expression of RAB11A normalized to GAPDH (mean ± SD)
0.025
0.020
0.015
0.010
0.005
0.000
**
**
***
RAB11A
β-actin
Relative expression of miR-631 normalized to 5S rRNA (mean ± SD)
0.010
0.008
0.006
0.0010
0.0005
0.0000
**
**
**
Control
2
4
6
pmiR-631 (ug)
C
Relative expression of RAB11A normalized to GAPDH (mean ± SD)
0.020
0.015
0.010
0.005
0.000
**
RAB11A
β-actin
Relative expression of miR-631 normalized to 5S rRNA (mean±SD)
0.04
0.03
0.02
0.01
0.00
*
Control
5-Aza

Fig 2

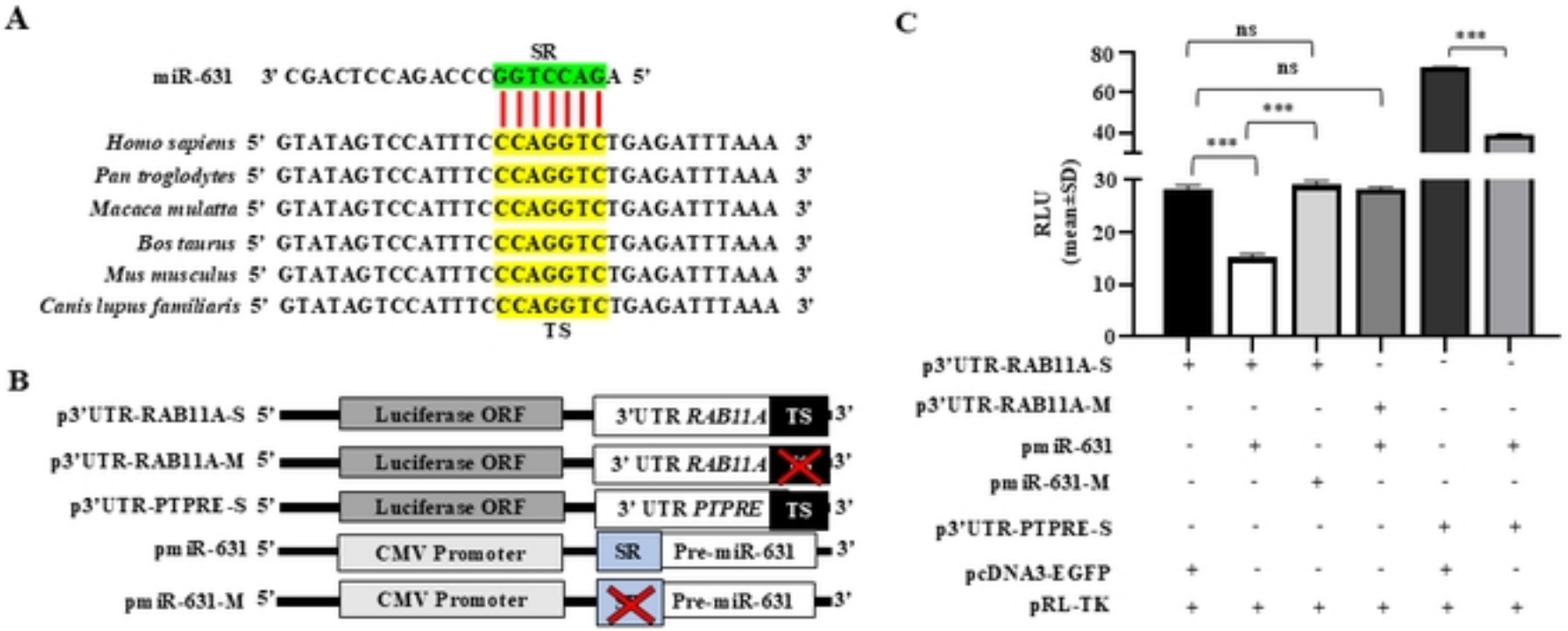
A
SR
miR-631 3' CGACTCCAGACCCGGTCCAGA 5'
Homo sapiens 5' GTATAGTCCATTTCCCAGGTCTGAGATTTAAA 3'
Pan troglodytes 5' GTATAGTCCATTTCCCAGGTCTGAGATTTAAA 3'
Macaca mulatta 5' GTATAGTCCATTTCCCAGGTCTGAGATTTAAA 3'
Bos taurus 5' GTATAGTCCATTTCCCAGGTCTGAGATTTAAA 3'
Mus musculus 5' GTATAGTCCATTTCCCAGGTCTGAGATTTAAA 3'
Canis lupus familiaris 5' GTATAGTCCATTTCCCAGGTCTGAGATTTAAA 3'
TS
B
p3'UTR-RAB11A-S 5' Luciferase ORF 3'UTR RAB11A TS 3'
p3'UTR-RAB11A-M 5' Luciferase ORF 3' UTR RAB11A 3'
p3'UTR-PTPRE-S 5' Luciferase ORF 3' UTR PTPRE TS 3'
pmiR-631 5' CMV Promoter SR Pre-miR-631 3'
pmiR-631-M 5' CMV Promoter Pre-miR-631 3'
C
RLU (mean±SD)
80
60
40
30
20
10
0
ns
ns
***
***
***
p3'UTR-RAB11A-S + + + - - -
p3'UTR-RAB11A-M - - - + - -
pmiR-631 - + - + - +
pmiR-631-M - - + - - -
p3'UTR-PTPRE-S - - - - + +
pcDNA3-EGFP + - - - + -
pRL-TK + + + + + +

Fig 3

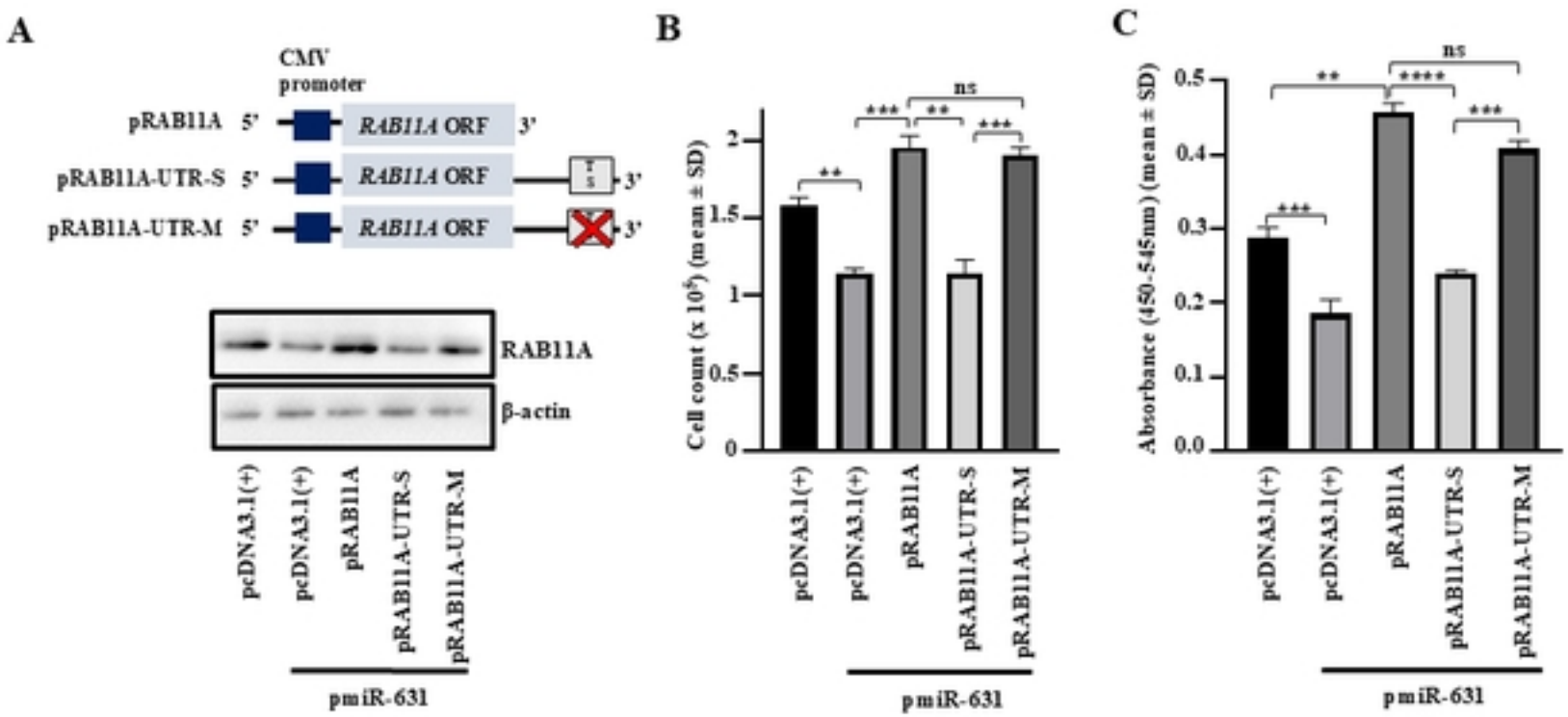
A
CMV promoter
pRAB11A 5'
RAB11A ORF
3'
pRAB11A-UTR-S 5'
RAB11A ORF
3'
pRAB11A-UTR-M 5'
RAB11A ORF
3'
RAB11A
β-actin
pcDNA3.1(+)
pcDNA3.1(+)
pRAB11A
pRAB11A-UTR-S
pRAB11A-UTR-M
pmiR-631
B
Cell count (x 10^6) (mean ± SD)
0
0.5
1
1.5
2
**
***
**
ns
***
pcDNA3.1(+)
pcDNA3.1(+)
pRAB11A
pRAB11A-UTR-S
pRAB11A-UTR-M
pmiR-631
C
Absorbance (450-545nm) (mean ± SD)
0.0
0.1
0.2
0.3
0.4
0.5
***
**
****
ns
***
pcDNA3.1(+)
pcDNA3.1(+)
pRAB11A
pRAB11A-UTR-S
pRAB11A-UTR-M
pmiR-631

Fig 4

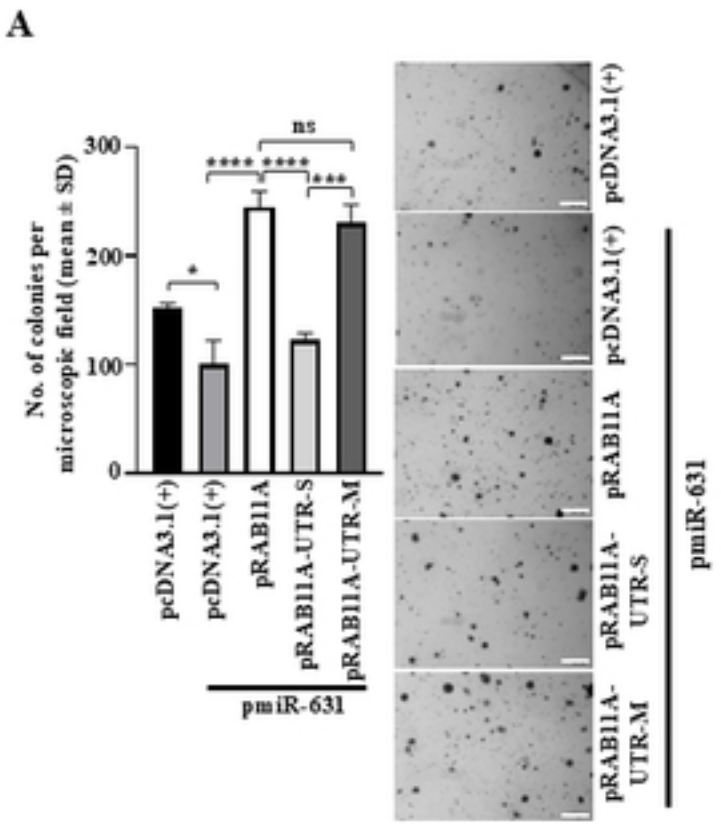
A
No. of colonies per microscopic field (mean ± SD)
300
200
100
0
*
****
****
ns
***
pcDNA3.1(+)
pcDNA3.1(+)
pRAB11A
pRAB11A-UTR-S
pRAB11A-UTR-M
pmiR-631
pcDNA3.1(+)
pcDNA3.1(+)
pRAB11A
pRAB11A-UTR-S
pRAB11A-UTR-M
pmiR-631

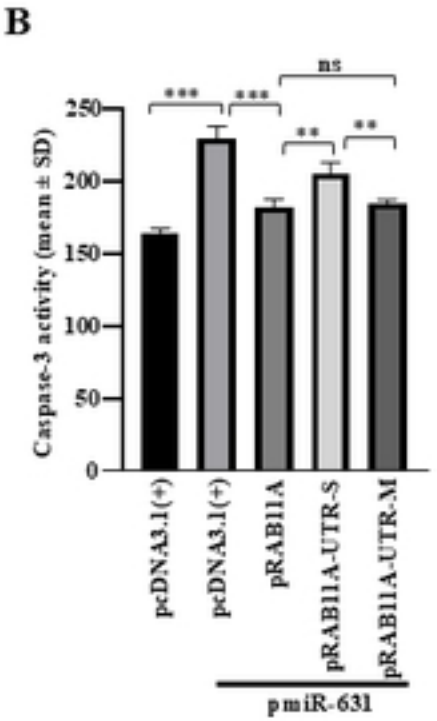
B
Caspase-3 activity (mean ± SD)
250
200
150
100
50
0
***
***
ns
**
**
pcDNA3.1(+)
pcDNA3.1(+)
pRAB11A
pRAB11A-UTR-S
pRAB11A-UTR-M
pmiR-631

Fig 5

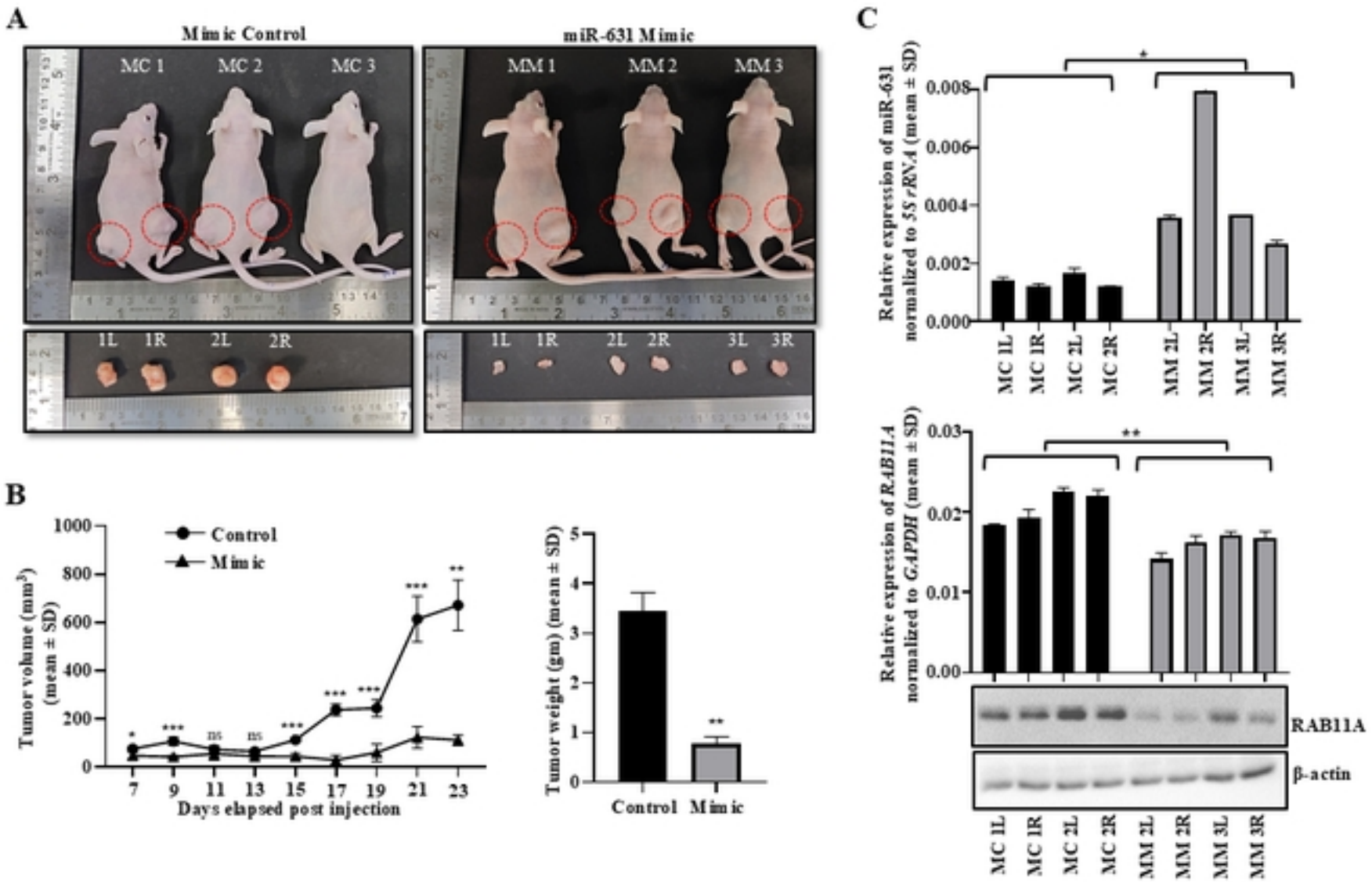
A
Mimic Control
miR-631 Mimic
MC 1
MC 2
MC 3
MM 1
MM 2
MM 3
1L
1R
2L
2R
3L
3R
B
Control
Mimic
Tumor volume (mm³) (mean ± SD)
Days elapsed post injection
Tumor weight (gm) (mean ± SD)
Control
Mimic
C
Relative expression of miR-631 normalized to 5S rRNA (mean ± SD)
Relative expression of RAB11A normalized to GAPDH (mean ± SD)
RAB11A
β-actin
MC 1L
MC 1R
MC 2L
MC 2R
MM 2L
MM 2R
MM 3L
MM 3R

Fig 6